Science Translational Medicine AAAS

Submitted Manuscript: Confidential template updated: February 28 2012

Title: **NexGen EBA: fourteen-day PET/CT changes identify synergies and antagonisms among anti-tuberculosis medications**

Authors: Yingda L. Xie[1], Veronique R. de Jager[2], Ray Y. Chen[3,10], Lori E. Dodd[4], Praveen Paripati[6], Laura E. Via[3,10], Dean Follmann[4], Jing Wang[5], Keith Lumbard[5], Saher Lahouar[6], Stephanus Malherbe[7], Jenna Andrews[8], Xiang Yu[3], Lisa Goldfeder[3], Ying Cai[3], Kriti Arora[3], Andre G. Loxton[7], Naadira Vanker[2], Michael Duvenhage[5], Jill Winter[9], Taeksun Song[10], Gerhard Walzl[7], Andreas Diacon[2,11], Clifton E. Barry, III[3,10]*

Affiliations:

[1]Division of Infectious Diseases, Department of Medicine, Rutgers New Jersey Medical School, Newark, NJ, USA

[2]TASK Applied Science, Cape Town, South Africa

[3]Tuberculosis Research Section, Laboratory of Clinical Immunology and Microbiology, Division of Intramural Research, National Institute of Allergy and Infectious Disease, National Institutes of Health, Bethesda, Maryland, USA

[4]Biostatistics Research Branch, Division of Clinical Research, National Institute of Allergy and Infectious Disease, National Institutes of Health, Bethesda, Maryland, USA

[5]Clinical Monitoring Research Program Directorate, Frederick National Laboratory for Cancer Research, Frederick, Maryland, USA

[6]Imaging Group, NET ESolutions Inc., McLean, Virginia, USA

[7]DST-NRF Centre of Excellence for Biomedical Tuberculosis Research, South African Medical Research Council Centre for Tuberculosis Research, Division of Molecular Biology and Human Genetics, Department of Biomedical Sciences, Faculty of Medicine and Health Sciences, Stellenbosch University, Cape Town, South Africa

[8]Microbial Pathogenesis, Yale University, New Haven, Connecticut, USA

[9]Catalysis Foundation for Health, San Ramon, California, USA

[10]Institute of Infectious Disease and Molecular Medicine, University of Cape Town, Cape Town, South Africa

[11]Department of Medicine, Stellenbosch University, Cape Town, South Africa

One Sentence Summary: FDG PET/CT adds significant information to microbiology in standard first in patient testing of tuberculosis medications.

Abstract: Early bactericidal activity (EBA) studies monitor daily bacterial counts in patients during 14 days of experimental treatment and are considered a critical step in new drug

development for tuberculosis (TB). The rate of change in sputum bacterial load over time provides an informative, but imperfect, estimate of drug activity. In this study, 160 participants received first-line chemotherapy and moxifloxacin individually and in combination. In addition to standard bacterial enumeration, participants received [^{18}F]Fluoro-2-deoxy-2-D-glucose positron emission tomography and computerized tomography ([^{18}F]FDG-PET/CT) at the beginning and end of the 14-day treatment period. Quantitation of the radiologic responses provided insights about single and combination drug activity across various lesion types and correlated better with established clinical outcomes than traditional sputum colony forming unit measurements alone. The radiologic data provides clear evidence of synergy between isoniazid and pyrazinamide and demonstrate that the activity of pyrazinamide is limited to lesions showing the highest FDG uptake.

Introduction

New drugs and improved drug regimens for treating tuberculosis (TB) are urgently needed to combat emerging resistance, decrease mortality and morbidity rates, and shorten therapy *(1, 2)*. The current six-month, four-drug regimen was defined in a pivotal series of clinical trials by the British Medical Research Council (BMRC) from 1946 to 1976 *(3)*. These trials relied on disease relapse as their primary endpoint, recognizing that patients had to be treated for months after their sputum culture conversion to avoid relapsing with active disease. The standard of care in the 1950s was 18 months of treatment with isoniazid and thiacetazone with daily streptomycin injections for the first two months. The first breakthrough in treatment duration occurred when rifampicin or pyrazinamide was added to streptomycin and isoniazid to achieve relapse rates of 3% and 8%, respectively, with only 6 months of therapy *(4)*. Through a series of additional trials, six-month therapy using both rifampin and pyrazinamide became established as the standard treatment duration for drug-sensitive TB, with relapse rates around

1%. Regimens that shortened to less than six months, even those that combined rifampin and pyrazinamide, had increasing rates of relapse *(5)*.

Remarkably, since this era of BMRC trials more than 40 years ago, this 6-month 1st-line regimen has not changed in composition or duration despite the advent of new drugs and resurgence in the global burden of TB. To accelerate identification of clinically effective drug candidates, better methodologies are needed to determine the best combinations of drugs to take forward into lengthy and resource-intensive clinical trials of durable cure. In TB drug development, investigators attempt to monitor bacterial counts quantitatively in the sputum of TB patients as an early indication of drug activity *(6)* and triage which regimens should proceed to expensive Phase 3 trials. The pioneering work of Jindani and Mitchison *(7)* applied this approach to new combinations of drugs and formalized the methodology called the early bactericidal activity (EBA) study. This methodology has become part of the US FDA official guidance documents for development of new TB drugs *(8)*. Despite the pivotal role of EBA trials in new drug development, this methodology has limitations. Important sterilizing drugs marked by capacity to shorten therapy and prevent relapse like rifampicin and pyrazinamide have only small EBA effects, while less sterilizing agents like isoniazid consistently perform very well. The only agents to date that have shown EBA on par with that of isoniazid were the fluoroquinolones, particularly moxifloxacin *(9–11)*. Data from mouse models suggesting strong sterilizing potential *(12–14)* and some observations of 8-week culture conversion rates in humans *(15–17)* formed the evidence for launching three Phase 3 trials based on using a fluoroquinolone to shorten the duration of TB chemotherapy for drug-sensitive disease to four months *(18–20)*. These trials all failed to show non-inferiority of four-month fluoroquinolone regimens to the six-month standard of care regimen based on disease relapse. The inherent limitation in examining

only sputum bacterial clearance is that this measure reflects only disease in the airways, not the parenchymal nodules, infected lymph nodes and other pulmonary disease pathologies characteristic of adult pulmonary TB.

We previously reported 2-deoxy-2-[^{18}F]fluoro-D-glucose (FDG)-PET/CT changes in two cohorts of patients: one small cohort with multi-drug resistant disease imaged at baseline and after two months of treatment *(21)*, and one larger cohort in drug-susceptible patients imaged at baseline, one month, and end of treatment *(22)*. In both cohorts, we saw significant changes in radiologic features, particularly in hard and total disease volume on CT and total glycolytic activity (mean standard uptake values of FDG x total volume) on PET, with successful treatment. In non-human primates experimentally infected with *Mycobacterium tuberculosis* (Mtb), we distinguished the 6-month sterilizing regimen of isoniazid, rifampicin, pyrazinamide, and ethambutol from a regimen that required 18 months of isoniazid and streptomycin in as little as two weeks using FDG-PET/CT changes *(23)*. We therefore postulated that we should be able to see significant changes in FDG-PET/CT features within a 14-day EBA study that would reveal more about the lesion-specific activity of individual drugs which have been clinically well-characterized in TB patients. We conducted an EBA study with the addition of FDG-PET/CT scans ('NexGen EBA'; NCT02371681) before and after 14 days of treatment among 160 pulmonary TB patients randomized across eight arms: four monotherapy arms using isoniazid, rifampicin, pyrazinamide, and moxifloxacin; two dual-agent combination arms: pyrazinamide-isoniazid and pyrazinamide-rifampicin; and two four-drug arms: isoniazid-rifampicin-pyrazinamide-ethambutol and moxifloxacin-rifampicin-pyrazinamide-ethambutol.

Results

Study Population and Baseline Characteristics

From December 2015 to September 2017, 178 eligible participants with HIV-negative sputum smear-positive pulmonary tuberculosis were enrolled at TASK Applied Science in the Western Cape region of South Africa. Eighteen of the 178 participants were withdrawn from the study (detailed in **Figure 1A**). The remaining 160 participants completed the study and were included in the overall study analysis. At baseline, there were no significant differences by arm in age, sex, body mass index (BMI), and sputum bacterial burden as approximated by Xpert MTB/RIF cycle threshold, the number of Mtb colony-forming units (CFU) on culture, or the PET/CT disease burden (ANOVA, P=0.34-0.9, **Table S1**). Total dense lesion volume and cavity airspace volume on CT were comparable by arm, with large inter-individual variability.

Early Bactericidal Activity

Early bactericidal activity by sputum CFU enumeration on agar plates (**Figure 2A**) as well as time-to-positivity (TTP) in broth culture, according to the mycobacterial growth indicator tube system (BACTEC MGIT 960), was highest for the moxifloxacin-rifampicin-pyrazinamide-ethambutol arm and lowest for the pyrazinamide arm (**Figure S1**). Among the single-drug arms, moxifloxacin showed the most robust response. There were no statistically significant differences between the EBA for rifampicin-pyrazinamide, isoniazid-rifampicin-pyrazinamide-ethambutol, isoniazid-pyrazinamide, and moxifloxacin arms or the EBA for the rifampicin and isoniazid arms (**Figure 2A**). At the participant level, intra-arm variability in the estimated EBA was observed (**Figure 2B**) and revealed the largest number of participant increases in bacterial load amongst those randomized to pyrazinamide, relative to the other arms. Notably, in 6 out of 8 arms there were individual participants who had increasing sputum CFU over 14 days. This

was most prominent in the pyrazinamide monotherapy arm with 8 of 19 (42%) participants showing an increase.

Radiologic measures

Among the 160 participants analyzed, two participants were excluded for the radiologic analysis: one had no intrapulmonary abnormalities on baseline PET/CT scan and the other had FDG incorrectly administered (likely due to intravenous line infiltration) at the day 14 scan. The remaining 158 participants yielded 1,122 total PET/CT features including "lesion" features, lung tissue with radiodensity from -500 to +200 Hounsfield units (HU) (N=802 lesions), and "cavitary air" features, radiodensity within pulmonary cavities from -1,024 to -500 HU (N=320). Lesions were defined as all abnormalities that occurred within a bronchopulmonary segment. If multiple adjacent segments were involved, abnormalities within those segments were considered one lesion. For example, in **Figure 1B** and **C,** this subject had three features: one complex lesion involving all five segments of the left superior lobe (green), one cavitary airspace within the apical region of that lesion (red), and one lesion confined to the left inferior lobe segment S6 (yellow). As expected, abnormalities were predominantly located in the upper regions of the lungs with more than half in either lung involving the apical bronchopulmonary segments S1 and S2 and 20-25% involving the apical segment of the lower lobe, S6 (**Figure S2**).

Lesion-level analysis

We excluded 45 abnormalities (39 "lesions" and 6 "cavitary air") in 34 participants from the analysis due to: lesion inactive with no FDG uptake and obvious calcification (n=13), severe segmental or lobar collapse (n=13), pleural lesion or effusion (n=7), new lesion at day 14 that

was completely absent from bronchopulmonary segment at baseline (n=7, rationale explained in next paragraph), severe reconstruction artifact (n=4), and accidental duplication of lesion (n=1) (**Table S2**). An arm-level overall analysis of the PET/CT lesion measures including change in total lesion volume, total glycolytic activity (TGA), and cavitary air are shown in **Figure 3A, B** and **Figure S3**, respectively. Cavity air was the most variable of these measurements across 14 days of treatment with 6 of 8 arms achieving reductions in air volume of 25-45%. At the single-drug arm level, rifampicin was the most active (compared to isoniazid, pyrazinamide, and moxifloxacin). All arms containing rifampicin showed large reductions in both lesion volume and inflammation (as measured by TGA). Moxifloxacin as a single agent also performed well. Isoniazid and pyrazinamide by themselves had the least effect, with pyrazinamide actually associated with an increase in mean lesion volume and inflammation over 14 days. Surprisingly, isoniazid and pyrazinamide were synergistic when combined, with changes similar to rifampicin alone or the combination isoniazid-rifampicin-pyrazinamide-ethambutol. The combination of rifampicin-pyrazinamide appeared slightly less active than rifampicin alone though this difference was not statistically significant in the lesion-level analysis. Comparison of these groups at the sub-lesion level is discussed with Figure 4, below.

New or expanding lesions (≥1 mL) were identified 97 times in 58 participants at day 14. Most of these were progressions of existing lesions into previously uninvolved areas of a bronchopulmonary segment but in a few cases new lesions appeared in a previously uninvolved lung segment. These new or expanding lesions occurred in all arms but more frequently in the isoniazid and pyrazinamide arms (**Figure S4**). In 35 of these participants there was an obvious direct bronchial connection with an active cavity either directly superior to the new or expanding lesion, or in the opposite lung, consistent with direct bronchial spread of existing disease.

Endobronchial spread has been well documented in the older pathology literature as a component of the natural history of pulmonary tuberculosis *(24–29)*. We studied this in more detail in a cohort of patients with extensive follow-up and also found that such lesions do not necessarily impact treatment outcome (**manuscript submitted**). Seven new lesions were excluded from this analysis (listed in **Table S2**) as they were in a completely new segment, and thus had no baseline reference for comparison. The remainder were included with the lesion from which they expanded and were included in the primary analysis.

Sub-lesion level analysis

The lesion-level analysis was also complicated by the heterogeneity of lesions that often spanned multiple bronchopulmonary segments. Even when a lesion was within a single segment, there were often heterogeneous local changes within a lesion. To isolate drug effects on specific subtypes of abnormalities, we computationally divided the dataset into 145,447 cubes of approximately 1 cm^3 from the original 802 non-cavity air lesions. We then aligned the baseline and day 14 cubes and calculated the properties of the voxels contained in these cubes at both visits (**Figure 1D** and **Figure S5**). Of these cubes, 18,760 (12.9%) had no density over -500 HU or FDG uptake at baseline. These represented new lesions that emerged during the study and were omitted from this analysis (**Figure S6**). The remaining 126,687 (87.1%) cubes were used to explore two specific features suggested by the primary analysis – the synergy of isoniazid and pyrazinamide and the antagonism of rifampicin and pyrazinamide.

To determine the interaction between isoniazid and pyrazinamide, we used linear mixed effects modelling to estimate the change in mean HU for all cubes in the isoniazid, pyrazinamide, and isoniazid-pyrazinamide arms (see statistical methods and **Supplemental Statistics**). Isoniazid-pyrazinamide was significantly more effective at reducing HUmean than

expected from the additive effect of isoniazid and pyrazinamide alone (P <0.05) (Figure **4A**). We also analyzed the cubes following stratification for FDG uptake into "hot" (mean standardized uptake value [SUVmean] >2) and "cold" (SUVmean <=2) categories. Isoniazid and pyrazinamide showed greater than additive decreases in HUmean in both categories of lesion cubes (P <0.05, Figure **4B**). In the case of rifampicin and pyrazinamide, the effect of combining the two was slightly less than additive (Figure **4C**). This apparent antagonism of rifampicin and pyrazinamide was affected by the baseline FDG-uptake of the cube; lesions that were "cold" at baseline showed the expected additive value for decreasing HUmean while lesions that were "hot" at baseline showed significantly less than additive decrease in HUmean (P <0.05, Figure **4D**).

The activity of pyrazinamide is linked to baseline inflammatory status of lesions.

Most participants in the pyrazinamide arm had a mixed response, with some lesions progressing while other lesions showed large reductions in volume and FDG-avidity. An example is shown in Figure **5A** where a participant with a left superior lobe cavity shows a large consolidation throughout the upper lobe that resolves 42% of the hard volume and 41% of the total glycolytic activity after 14 days of pyrazinamide treatment. At the same time, a smaller nodular area of disease in the left inferior lobe worsens by 600% over the same time interval in both hard volume and TGA. Twelve of the 19 participants in the pyrazinamide arm showed signs of progression in lesions from baseline to day 14. Closer inspection of the lesion features that responded to pyrazinamide treatment revealed that response was directly related to the degree of inflammation at baseline. To understand the variability of lesion responses to pyrazinamide, we examined the properties of all cubes embedded in these participants' lesions. Because this

appeared to be related to total lesion density more than simple HUmean, we also calculated the total lesion mass (TLM) by summing the values of individual voxels within cubes after adding 1,024 to each (to normalize to positive numbers for negative HU values, with -1,024 being the minimum value in the dataset; TLM = lesion volume x [1024 + mean HU of lesion voxels]) as well as calculating total glycolytic activity for each cube. Changes in those four cube properties were then analyzed stratified by the baseline SUVmean from 0 to 10. Thus, cubes that had a baseline SUVmean of 0-1 (the bottom row of **Figure 5B**) worsened significantly in terms of all four properties. We found that cubes that responded to pyrazinamide had baseline SUVmean values above 5, while lesions that progressed had SUVmean values below 3 (**Figure 5B**). This pattern of response was unique to pyrazinamide as other monotherapies showed no such pattern (**Figure S7**).

Discussion

Two-week monotherapy studies in subjects with active TB are recommended by the US Food and Drug Administration, and the European Medicines Agency as a necessary part of the development process for new antituberculosis agents *(8, 30–32)*. The risk of developing drug-resistance to the agents has been shown to be very low and such studies are widely accepted *(8, 30–32)*. Our EBA CFU data were broadly in line with prior reports. Our 14-day EBA estimate for isoniazid was 0.1 whereas other studies found it to be 0.19 *(33)*. Our EBA estimate for rifampicin was in line with what has been reported previously and similar to isoniazid in our study. The negligible EBA of pyrazinamide has also been previously confirmed *(7, 34)*. Our estimate for the 14-day EBA of moxifloxacin of 0.14 is slightly lower than the previously reported 0.17 for the 2-7 day EBA *(10)*. Our EBA for isoniazid-rifampicin-pyrazinamide-

ethambutol was 0.14, in line with a recent meta-analysis of EBA studies where it ranged from 0.1 to 0.2 *(35)*. Scant prior 14-day EBA data are available for the combinations isoniazid-pyrazinamide (only four patients in one prior report) or rifampicin-pyrazinamide, or for the four-drug combination moxifloxacin-rifampicin-pyrazinamide-ethambutol.

Our PET-CT data showed that at an aggregate lesion level, rifampicin and moxifloxacin were the most effective in achieving reductions in mean lesion volume and TGA. Pyrazinamide and isoniazid by contrast had small or negative effects on both lesion volume and TGA. Whereas isoniazid is superior to rifampicin in conventional sputum CFU reduction, its clear inferiority to rifampicin in reducing lesion volume and inflammation radiologically suggests that the radiology results are more in line with the actual clinical performance of these agents. Although as single agents isoniazid and pyrazinamide were the least active in the aggregate PET-CT data, the combination of the two synergistically reduced both lesion volume and TGA similar to rifampicin.

In addition, rifampicin by itself had the highest reduction in lesion volume, slightly higher than every combination arm within which it appeared. However, it is worth noting that the 14-day EBA period is intended to precede the effects of drug resistance and tolerance with monotherapy that develop over time. Therefore, this model cannot be used to identify monotherapies for TB, but rather to capture the contribution of each drug to inform the rational design of combination regimens in early Phase II studies that would still need to be validated against clinical outcomes. Meanwhile the superiority of rifampin alone to all other arms that contain pyrazinamide suggested a potentially unrecognized antagonism between rifampicin and pyrazinamide. The effects of combining isoniazid and pyrazinamide, as well as rifampicin and pyrazinamide, were not directly evaluated in the original BMRC clinical trials as both agents

were introduced onto a backbone of isoniazid and streptomycin and never tested together without isoniazid. However, their effects may be indirectly inferred from additions and subtractions of these drugs to the same background regimen. Specifically, in the 1970 short course chemotherapy studies in East and Central Africa, the addition of pyrazinamide to streptomycin and isoniazid for 6 months lowered the relapse rate from 29% to 8% compared with 6 months of isoniazid-streptomycin alone, suggesting a potent effect of adding pyrazinamide to isoniazid *(4)*. Additionally, while there were no comparisons of rifampicin-pyrazinamide with rifampicin and pyrazinamide individually in the initial 2 months of therapy, the use of isoniazid-rifampicin-pyrazinamide compared with isoniazid-rifampicin or isoniazid-pyrazinamide in the 4-month continuation phase (with the same 2 month intensive phase regimen isoniazid-rifampicin-pyrazinamide-streptomycin) led to a 16% rate of relapse compared with 11% with isoniazid-rifampicin and 32% with isoniazid-pyrazinamide *(36, 37)*. The lack of activity of pyrazinamide in the continuation phase was notable and the slightly higher relapse rate when pyrazinamide was used in combination with rifampicin are consistent with our observations that pyrazinamide is uniquely active in the highly inflamed state occurring early in treatment. Mitchison has long argued that the clinical effect of pyrazinamide being limited to the first two months of therapy suggests that its activity is directly associated with inflammation *(38)*. Our lesion-level analysis proved insufficient to resolve some questions relating to smaller lesion features embedded within the complex TB lesions observed in these participants. To understand the effects of these drugs and combinations, we computationally divided these lesions into cubes of about 1 cubic centimeter and co-aligned these between baseline and day 14. The resulting comparisons offered further support for the observed synergy between isoniazid and pyrazinamide and the observed antagonism between rifampicin and pyrazinamide. It also allowed us to further understand the

impact of pyrazinamide on lesions. Cubes within lesions that respond to pyrazinamide monotherapy had notably higher SUVmean than cubes within lesions which did not respond or which worsened. Our understanding of the role neutrophils play in TB disease has altered recently with the demonstration that neutrophils represent the predominant cell type in human sputum *(39)* and the dominance of a gene signature associated with neutrophils in the peripheral blood of patients with active disease that wanes upon treatment *(40)*. The relationship between lesion reduction with pyrazinamide and areas of high glucose uptake suggests that the inflammation associated with pyrazinamide activity may represent areas rich in neutrophils. The acidic pH required for pyrazinamide activity may then arise from neutrophil myeloperoxidase *(41)*. This may also explain why the activity of pyrazinamide tapers after the first 2 months of treatment, correlating with a decline in neutrophilic and inflammatory burden.

It was also evident from analysis of the lesion cubes that the synergy seen between isoniazid and pyrazinamide was most pronounced in lesions that were "cold" at baseline. One possible explanation for this could be that isoniazid, being a bacteriolytic agent, enhances the neutrophil recruitment to these lesions by causing antigen release from killed bacteria, and thereby enhancing pyrazinamide's effects. Conceivably, this "boosting" effect was most pronounced in cold lesions that would have otherwise shown little response to pyrazinamide without isoniazid's inflammatory recruitment. Likewise, the basis for the antagonism of the combination of rifampicin and pyrazinamide could be that rifampicin, which inhibits bacterial transcription, acts as an anti-inflammatory by shutting down the production of antigen driving neutrophil recruitment. This would explain why this antagonism is limited to lesion areas that are hot at baseline since pyrazinamide would have killing activity in the presence of neutrophils in only those lesion areas. Together, these data suggest the intriguing hypothesis that the unique

sterilizing activity of pyrazinamide may be related to neutrophil-induced acidification in a subset of TB lesions.

Finally, our comparison of the four-drug regimen moxifloxacin-rifampicin-pyrazinamide-ethambutol that failed to shorten the duration of treatment (despite improved sputum bacterial clearance) compared to the standard four-drug treatment isoniazid-rifampicin-pyrazinamide-ethambutol in the REMox trial *(18)*, revealed no advantage of moxifloxacin-rifampicin-pyrazinamide-ethambutol in reducing lesion volume or inflammation. These data are consistent with the clinical data showing four months of treatment with moxifloxacin-rifampicin-pyrazinamide-ethambutol is inadequate to achieve durable cure. In contrast to this, our PET/CT data (Figures 3A and 3B) suggest that single drug treatment with rifampin or moxifloxacin may be as effective as standard four-drug treatment isoniazid-rifampicin-pyrazinamide-ethambutol. Our data does suggest that the antagonistic activity of pyrazinamide on the efficacy of rifampicin may limit the short-term sterilizing potential of the four drug combination but this serves to highlight an inherent limitation of two-week EBA studies, which are unable to assess factors such as emergence of drug-resistance and sub-populations of lesions that may respond differentially to individual agents. This is why results from EBA studies still need to be validated in longer, later phase trials.

Our data explain three important clinical observations. First, the observation that pyrazinamide only exerts an effect during the first two months of treatment is explained by our finding that the activity of pyrazinamide is limited to lesions with high baseline inflammation. After the first month of therapy, inflammation is substantially reduced as measured in our previous 1-month PET/CT study *(22)*. Second, the observation that adding either pyrazinamide or rifampicin to a backbone of isoniazid and streptomycin was enough to shorten therapy to six

months but adding both did not allow further treatment shortening is explained by the antagonism between pyrazinamide and rifampicin when given together. Third, the failure of moxifloxacin-rifampicin-pyrazinamide-ethambutol to shorten therapy is explained by our data showing that despite more rapid sputum clearance of bacteria by this combination, the underlying pathology resolves at the same rate as with the standard isoniazid-rifampicin-pyrazinamide-ethambutol. These observations would not have been possible without detailed analyses of the PET/CT scans, which allowed the heterogeneous responses of different drugs on different TB lesions to be quantitated and teased apart. Our study shows that PET/CT changes, such as lesion volume and PET activity, within a short timeframe are a valuable early drug evaluation tool to characterize individual and combinations of agents and understand the differential effects of these agents on specific pathological manifestations of disease. Understanding these effects for new agents and combinations will facilitate the design of rational drug regimens that can achieve sterile cure in a shorter duration.

Materials and Methods

Study Design and Participants

Ethics approval was obtained from the National Institute of Allergy and Infectious Diseases institutional review board, the Stellenbosch University Human Research Ethics Committee, and the South African Health Products Regulatory Authority. We performed a partially blinded (laboratory personnel, scan readers, and statisticians were blinded to arm assignment), randomized trial evaluating 14-day EBA, FDG-PET/CT changes, and immunologic and bacterial markers to distinguish responses to standard TB drugs which have been characterized by clinical outcomes and pharmacokinetic data over their 40-60 years of use. HIV-negative individuals with

sputum smear microscopy-positive, Xpert MTB/RIF positive, pulmonary tuberculosis and abnormal chest X-ray findings were enrolled into the study (full inclusion/exclusion criteria in Supplementary **Table S3**). After informed consent, eligible participants were randomized to one of eight treatment arms, including four single-drug arms (isoniazid, rifampicin, pyrazinamide, and moxifloxacin), two 2-drug arms (rifampicin-pyrazinamide and isoniazid-pyrazinamide) and two 4-drug arms (moxifloxacin-rifampicin-pyrazinamide-ethambutol and isoniazid-rifampicin-pyrazinamide-ethambutol). All participants received directly observed treatment for 14 consecutive days in a monitored inpatient setting at the TASK Applied Science Clinical Trial Centre, a registered research hospital, in Cape Town, South Africa. Participants were assigned a study-generated participant identification code ensuring anonymity. Treatment assignment used centrally generated randomization codes in sequentially numbered envelopes maintained by the study pharmacist. All participants underwent a PET/CT scan at pre-treatment baseline (day -2 ±1 day window) and day 14 (±3 day window) of treatment, in addition to daily overnight sputum sample collection for traditional early bactericidal activity measurements. Safety assessments included daily history, vital signs, physical examination, and monitoring for adverse events; the latter also comprised full blood counts, coagulation studies, clinical chemistry, and urinalysis. The isoniazid-rifampicin-pyrazinamide-ethambutol arm alone was treated to day 28, with additional sputum, blood, and PET/CT scan collected at that time to allow comparison to other studies.

Sputum CFU (Early Bactericidal Activity) and Time to Positivity

Sputum specimens were collected for 16 hours overnight starting 2 days prior to treatment initiation and each day afterwards. Collections were terminated before administration of the next

day's therapy. Sputum for colony forming unit (CFU) counts of *Mtb* and measurement of time to positivity (TTP) in liquid culture medium (BACTEC MGIT 960, Becton Dickinson, Woodmead, South Africa) were subject to laboratory processing centrally at the TASK laboratory. *Mtb* speciation was done by PCR. Cultures from baseline and the last available overnight sputum collections were tested for susceptibility to first-line drugs (MGIT SIRE kit, Becton Dickinson) and to moxifloxacin (MGIT 960, Becton Dickinson). CFU data were interrogated using linear mixed effects modelling. The models, which aimed to quantify the effect of treatment regimen on bacteriological decline, were fit separately within each arm and included a fixed effect term for visit number and a random intercept term for subject. For each subject, his or her measured CFU values at each visit contributed to the estimate of EBA for the arm to which he or she belonged. Results were similar when using standard EBA estimation methods.

FDG-PET/CT

2-deoxy-2-[^{18}F]Fluoro-D-glucose (FDG) PET/CT exams were performed prior to administration of the first dose of study drug and immediately after the 14th daily dose. Participants fasted for at least 6 h before [^{18}F] FDG administration. According to body weight, 185–259 MBq of [^{18}F] FDG was administered intravenously 60 minutes before the scan. CT parameters were set at 120 kV, 200 mA (no dose modulation), 0.75 sec rotation time, pitch 0.438, and collimation 16x0.75mm. Investigators analyzing the PET/CTs were blinded to treatment arms.

PET/CT features were analyzed by grouping pulmonary abnormalities within a bronchopulmonary segment from all participants. We excluded obvious pleural effusions and

other extrapulmonary sites of infection. All abnormalities within the thoracic cavity were labelled by the bronchopulmonary segment(s) in which they were located and segmented manually as regions of interest ("ROI") using the 3D image analysis software Amira (versions 6.4.0 and 6.5.0, ThermoFisher Scientific). Each abnormality was defined as either "cavity air" features present within the pulmonary cavity from -1024 to -500 HU or "lesion" features that represented material with a radiodensity ranging from -500 to +200 Hounsfield units (HU). If multiple confluent segments were involved, abnormalities within all those segments were considered as one lesion. Every scan was read by two separate readers, then subjected to at least two rounds of quality control editing by a third reader for consistency, accuracy, and removal of normal structures including vasculature. For the sub-lesion analysis, each lesion was enclosed in the smallest axis-aligned rectangular volume of voxels. The voxels were grouped into 11x11x11 blocks, starting at the top left corner. Lesion voxels within each cube were then used to compute HU-based as well as SUV-based statistics (mean, standard deviation, etc.) for the cube. PET and CT scans were co-registered based on their global coordinates from the scan and PET values were assigned to CT voxels based on the PET voxel closest to the front, bottom, left corner of each CT voxel. Lesion voxel cubes were then co-registered between the baseline and day 14 scans.

Statistical analysis

Hypothesis testing comparing change from baseline to day 14 across treatment groups was undertaken at the cube-level. Cube values within a lesion are correlated as are lesions within a subject. To address this multi-level correlation, we fit linear mixed effects models with random effects for subject and for lesions nested within subject. Primary comparisons of interest were

based on changes of HUmean values for 1) isoniazid and pyrazinamide vs. isoniazid-pyrazinamide; and 2) rifampicin and pyrazinamide vs rifampicin-pyrazinamide, to evaluate whether the effect of the two-drug combination was synergistic, antagonistic or additive. Additional comparisons evaluated whether the HUmean changes between arms differed by baseline cube category of SUV-hot (SUVmean>2) vs SUV-cold (SUVmean<2). Estimation and hypothesis testing were conducted using the LMER and lmerTest packages in R version 3.5.3. P-values <0.05 were set to determine statistical significance. Full outputs for the LMER models are in **Supplemental Statistics**.

Supplementary Materials

Fig. S1. Estimated EBA effect from time-to-positivity of cultures from the cultures in liquid broth medium according to the mycobacterial growth indicator tube system (BACTEC MGIT 960).

Fig. S2. Segmental distribution of annotated lesions (including cavitary air).

Fig. S3. Cavitary air percent change by arm.

Fig. S4. Appearance of new or expanded lesions by study arm.

Fig. S5. Sub-lesion level analysis.

Fig. S6. Arm distribution of cubes that contained no lesion material at baseline.

Fig S7. Cube-level response to individual agents stratified by baseline SUVmean values

Table S1. Participant baseline characteristics.

Table S2. Lesions excluded from lesion-level analysis.

Table S3. Inclusion and exclusion criteria.

Supplemental statistical modeling methods.

References:

1. G. B. Gomez, D. W. Dowdy, M. L. Bastos, A. Zwerling, S. Sweeney, N. Foster, A. Trajman, M. A. Islam, S. Kapiga, E. Sinanovic, G. M. Knight, R. G. White, W. A. Wells, F. G. Cobelens, A. Vassall, Cost and cost-effectiveness of tuberculosis treatment shortening: a model-based analysis., *BMC Infect. Dis.* **16**, 726 (2016).

2. E. A. Kendall, S. Shrestha, T. Cohen, E. Nuermberger, K. E. Dooley, L. Gonzalez-Angulo, G. J. Churchyard, P. Nahid, M. L. Rich, C. Bansbach, T. Forissier, C. Lienhardt, D. W. Dowdy,

Priority-Setting for Novel Drug Regimens to Treat Tuberculosis: An Epidemiologic Model., *PLoS Med.* **14**, e1002202 (2017).

3. W. Fox, G. A. Ellard, D. A. Mitchison, Studies on the treatment of tuberculosis undertaken by the British Medical Research Council tuberculosis units, 1946-1986, with relevant subsequent publications., *Int. J. Tuberc. Lung Dis.* **3**, S231-79 (1999).

4. Controlled clinical trial of four short-course (6-month) regimens of chemotherapy for treatment of pulmonary tuberculosis. Third report. East African-British Medical Research Councils., *Lancet (London, England)* **2**, 237–40 (1974).

5. W. Fox, Whither short-course chemotherapy?, *Br. J. Dis. Chest* **75**, 331–57 (1981).

6. A. H. Diacon, P. R. Donald, The early bactericidal activity of antituberculosis drugs., *Expert Rev. Anti. Infect. Ther.* **12**, 223–37 (2014).

7. A. Jindani, V. R. Aber, E. A. Edwards, D. A. Mitchison, The early bactericidal activity of drugs in patients with pulmonary tuberculosis., *Am. Rev. Respir. Dis.* **121**, 939–49 (1980).

8. Food and Drug Administration, *Pulmonary Tuberculosis: Developing Drugs for Treatment* (2013; https://www.fda.gov/media/87194/download).

9. M. W. R. Pletz, A. De Roux, A. Roth, K.-H. Neumann, H. Mauch, H. Lode, Early bactericidal activity of moxifloxacin in treatment of pulmonary tuberculosis: a prospective, randomized study., *Antimicrob. Agents Chemother.* **48**, 780–2 (2004).

10. J. L. Johnson, D. J. Hadad, W. H. Boom, C. L. Daley, C. A. Peloquin, K. D. Eisenach, D. D. Jankus, S. M. Debanne, E. D. Charlebois, E. Maciel, M. Palaci, R. Dietze, Early and extended early bactericidal activity of levofloxacin, gatifloxacin and moxifloxacin in pulmonary tuberculosis., *Int. J. Tuberc. Lung Dis.* **10**, 605–12 (2006).

11. R. D. Gosling, L. O. Uiso, N. E. Sam, E. Bongard, E. G. Kanduma, M. Nyindo, R. W. Morris, S. H. Gillespie, The bactericidal activity of moxifloxacin in patients with pulmonary tuberculosis., *Am. J. Respir. Crit. Care Med.* **168**, 1342–5 (2003).

12. E. Miyazaki, M. Miyazaki, J. M. Chen, R. E. Chaisson, W. R. Bishai, Moxifloxacin (BAY12-8039), a new 8-methoxyquinolone, is active in a mouse model of tuberculosis., *Antimicrob. Agents Chemother.* **43**, 85–9 (1999).

13. E. L. Nuermberger, T. Yoshimatsu, S. Tyagi, R. J. O'Brien, A. N. Vernon, R. E. Chaisson, W. R. Bishai, J. H. Grosset, Moxifloxacin-containing regimen greatly reduces time to culture conversion in murine tuberculosis, *Am J Respir Crit Care Med* **169**, 421–426 (2004).

14. E. L. Nuermberger, T. Yoshimatsu, S. Tyagi, K. Williams, I. Rosenthal, R. J. O'Brien, A. A. Vernon, R. E. Chaisson, W. R. Bishai, J. H. Grosset, Moxifloxacin-containing regimens of reduced duration produce a stable cure in murine tuberculosis., *Am. J. Respir. Crit. Care Med.* **170**, 1131–4 (2004).

15. R. Rustomjee, C. Lienhardt, T. Kanyok, G. R. Davies, J. Levin, T. Mthiyane, C. Reddy, A. W. Sturm, F. A. Sirgel, J. Allen, D. J. Coleman, B. Fourie, D. A. Mitchison, T. B. study team Gatifloxacin for, A Phase II study of the sterilising activities of ofloxacin, gatifloxacin and moxifloxacin in pulmonary tuberculosis, *Int J Tuberc Lung Dis* **12**, 128–138 (2008).

16. M. B. Conde, A. Efron, C. Loredo, G. R. De Souza, N. P. Graca, M. C. Cezar, M. Ram, M.

A. Chaudhary, W. R. Bishai, A. L. Kritski, R. E. Chaisson, Moxifloxacin versus ethambutol in the initial treatment of tuberculosis: a double-blind, randomised, controlled phase II trial, *Lancet* **373**, 1183–1189 (2009).

17. S. E. Dorman, J. L. Johnson, S. Goldberg, G. Muzanye, N. Padayatchi, L. Bozeman, C. M. Heilig, J. Bernardo, S. Choudhri, J. H. Grosset, E. Guy, P. Guyadeen, M. C. Leus, G. Maltas, D. Menzies, E. L. Nuermberger, M. Villarino, A. Vernon, R. E. Chaisson, Tuberculosis Trials Consortium, Substitution of moxifloxacin for isoniazid during intensive phase treatment of pulmonary tuberculosis., *Am. J. Respir. Crit. Care Med.* **180**, 273–80 (2009).

18. S. H. Gillespie, A. M. Crook, T. D. McHugh, C. M. Mendel, S. K. Meredith, S. R. Murray, F. Pappas, P. P. J. J. Phillips, A. J. Nunn, REMoxTB Consortium, Four-month moxifloxacin-based regimens for drug-sensitive tuberculosis., *N. Engl. J. Med.* **371**, 1577–87 (2014).

19. C. S. Merle, K. Fielding, O. B. Sow, M. Gninafon, M. B. Lo, T. Mthiyane, J. Odhiambo, E. Amukoye, B. Bah, F. Kassa, A. N'Diaye, R. Rustomjee, B. C. de Jong, J. Horton, C. Perronne, C. Sismanidis, O. Lapujade, P. L. Olliaro, C. Lienhardt, A Four-Month Gatifloxacin-Containing Regimen for Treating Tuberculosis, *N. Engl. J. Med.* **371**, 1588–1598 (2014).

20. A. Jindani, T. S. Harrison, A. J. Nunn, P. P. J. Phillips, G. J. Churchyard, S. Charalambous, M. Hatherill, H. Geldenhuys, H. M. McIlleron, S. P. Zvada, S. Mungofa, N. A. Shah, S. Zizhou, L. Magweta, J. Shepherd, S. Nyirenda, J. H. van Dijk, H. E. Clouting, D. Coleman, A. L. E. Bateson, T. D. McHugh, P. D. Butcher, D. A. Mitchison, RIFAQUIN Trial Team, High-dose rifapentine with moxifloxacin for pulmonary tuberculosis., *N. Engl. J. Med.* **371**, 1599–608 (2014).

21. R. Y. Chen, L. E. Dodd, M. Lee, P. Paripati, D. A. Hammoud, J. M. Mountz, D. Jeon, N. Zia, H. Zahiri, M. T. Coleman, M. W. Carroll, J. D. Lee, Y. J. Jeong, P. Herscovitch, S. Lahouar, M. Tartakovsky, A. Rosenthal, S. Somaiyya, S. Lee, L. C. Goldfeder, Y. Cai, L. E. Via, S.-K. Park, S.-N. Cho, C. E. Barry, PET/CT imaging correlates with treatment outcome in patients with multidrug-resistant tuberculosis., *Sci. Transl. Med.* **6**, 265ra166 (2014).

22. S. T. Malherbe, S. Shenai, K. Ronacher, A. G. Loxton, G. Dolganov, M. Kriel, T. Van, R. Y. Chen, J. Warwick, L. E. Via, T. Song, M. Lee, G. Schoolnik, G. Tromp, D. Alland, C. E. Barry, J. Winter, G. Walzl, L. Lucas, G. V. D. Spuy, K. Stanley, L. Theart, B. Smith, N. Burger, C. G. G. Beltran, E. Maasdorp, A. Ellmann, H. Choi, J. Joh, L. E. Dodd, B. Allwood, C. Kogelenberg, M. Vorster, S. Griffith-Richards, Persisting positron emission tomography lesion activity and Mycobacterium tuberculosis mRNA after tuberculosis cure, *Nat. Med.* **22** (2016), doi:10.1038/nm.4177.

23. L. E. Via, K. England, D. M. Weiner, D. Schimel, M. D. Zimmerman, E. Dayao, R. Y. Chen, L. E. Dodd, M. Richardson, K. K. Robbins, Y. Cai, D. Hammoud, P. Herscovitch, V. Dartois, J. L. Flynn, C. E. Barry, A sterilizing tuberculosis treatment regimen is associated with faster clearance of bacteria in cavitary lesions in marmosets, *Antimicrob. Agents Chemother.* **59** (2015), doi:10.1128/AAC.00115-15.

24. G. CANETTI, Dynamic aspects of the pathology and bacteriology of tuberculous lesions., *Am. Rev. Tuberc.* **74**, 13–21; discussion, 22–7 (1956).

25. W. Pagel, Origin of Bronchogenic Tuberculosis in the Adult., *Br. Med. J.* **2**, 791 (1944).

26. E. M. MEDLAR, Pathogenetic concepts of tuberculosis., *Am. J. Med.* **9**, 611–22 (1950).

27. E. M. MEDLAR, The behavior of pulmonary tuberculous lesions; a pathological study., *Am. Rev. Tuberc.* **71**, 1–244 (1955).

28. A. R. Rich, *The Pathogenesis of Tuberculosis* (Charles C Thomas, Springfield, IL, 1st Edit., 1946).

29. G. G. Kayne, W. Pagel, L. O'Shaughnessy, *Pulmonary Tuberculosis: Pathology, Diagnosis, Management and Prevention* (Oxford University Press, London, 2nd Edit., 1948).

30. European Medicines Agency, *Draft addendum to the "guideline on the evaluation of medicinal products indicated for treatment of bacterial infections" to address the clinical development of new agents to treat disease due to Mycobacterium tuberculosis Revision 1* (2016; http://www.ema.europa.eu/docs/en_GB/document_library/Scientific_guideline/2016/08/WC500211447.pdf).

31. Global Alliance for TB Drug Development, Tuberculosis. Scientific blueprint for tuberculosis drug development., *Tuberculosis (Edinb).* **81 Suppl 1**, 1–52 (2001).

32. G. Davies, M. Boeree, D. Hermann, M. Hoelscher, Accelerating the transition of new tuberculosis drug combinations from Phase II to Phase III trials: New technologies and innovative designs., *PLoS Med.* **16**, e1002851 (2019).

33. P. R. Donald, A. H. Diacon, The early bactericidal activity of anti-tuberculosis drugs: a literature review., *Tuberculosis (Edinb).* **88 Suppl 1**, S75-83 (2008).

34. F. J. Botha, F. A. Sirgel, D. P. Parkin, B. W. van de Wal, P. R. Donald, D. A. Mitchison, Early bactericidal activity of ethambutol, pyrazinamide and the fixed combination of isoniazid, rifampicin and pyrazinamide (Rifater) in patients with pulmonary tuberculosis., *S. Afr. Med. J.* **86**, 155–8 (1996).

35. L. J. Bonnett, G. Ken-Dror, G. C. K. W. Koh, G. R. Davies, Comparing the Efficacy of Drug Regimens for Pulmonary Tuberculosis: Meta-analysis of Endpoints in Early-Phase Clinical Trials., *Clin. Infect. Dis.* **65**, 46–54 (2017).

36. Controlled clinical trial of five short-course (4-month) chemotherapy regimens in pulmonary tuberculosis. First report of 4th study. East African and British Medical Research Councils, *Lancet* **2**, 334–338 (1978).

37. Controlled clinical trial of five short-course (4-month) chemotherapy regimens in pulmonary tuberculosis. Second report of the 4th study. East African/British Medical Research Councils Study, *Am Rev Respir Dis* **123**, 165–170 (1981).

38. D. A. Mitchison, The action of antituberculosis drugs in short-course chemotherapy., *Tubercle* **66**, 219–25 (1985).

39. S.-Y. Eum, J.-H. Kong, M.-S. Hong, Y.-J. Lee, J.-H. Kim, S.-H. Hwang, S.-N. Cho, L. E. Via, C. E. Barry, Neutrophils are the predominant infected phagocytic cells in the airways of patients with active pulmonary TB., *Chest* **137**, 122–8 (2010).

40. M. P. R. Berry, C. M. Graham, F. W. McNab, Z. Xu, S. A. A. Bloch, T. Oni, K. A. Wilkinson, R. Banchereau, J. Skinner, R. J. Wilkinson, C. Quinn, D. Blankenship, R. Dhawan, J. J. Cush, A. Mejias, O. Ramilo, O. M. Kon, V. Pascual, J. Banchereau, D. Chaussabel, A. O'Garra, An interferon-inducible neutrophil-driven blood transcriptional signature in human

tuberculosis., *Nature* **466**, 973–7 (2010).

41. R. S. Rodrigues, F. A. Bozza, C. J. Hanrahan, L.-M. Wang, Q. Wu, J. M. Hoffman, G. A. Zimmerman, K. A. Morton, 18F-fluoro-2-deoxyglucose PET informs neutrophil accumulation and activation in lipopolysaccharide-induced acute lung injury., *Nucl. Med. Biol.* **48**, 52–62 (2017).

Funding: This research was supported in part by the Bill & Melinda Gates Foundation and in part by the Division of Intramural Research, National Institute of Allergy and Infectious Diseases, US National Institutes of Health. The findings and conclusions contained within are those of the authors and do not necessarily reflect positions or policies of the Bill & Melinda Gates Foundation. This project has additionally been funded from funds from the National Institutes of Health Contract No. 75N98119F00012 for Clinical Data Management System (CDMS). This project has been funded in whole or in part with federal funds from the National Cancer Institute, National Institutes of Health, under Contract No. 75N91019D00024, Task Order No. 75N91019F00130. The content of this publication does not necessarily reflect the views or policies of the Department of Health and Human Services, nor does mention of trade names, commercial products, or organizations imply endorsement by the U.S. Government. STM receives funding from the EDCTP2 program supported by the European Union (grant number CDF1576). The views and opinions of authors expressed herein do not necessarily state or reflect those of EDCTP.

Author contributions: CEB, YLX, RYC, LED designed and wrote the clinical protocol, AD, VRJ, SM, AGL, NV, GW supervised subject recruitment and testing, VRJ, LEV, LG, YC, KA, MD, JW, TS were responsible for regulatory oversight and data management, YLX, RYC, JA, CEB, PP, SL performed the primary analysis of radiological data, LED, DF, JW, KL, XY performed statistical analysis of data, CEB, RYC, YLX, DF, GW, AD wrote the manuscript.
Competing interests: None.

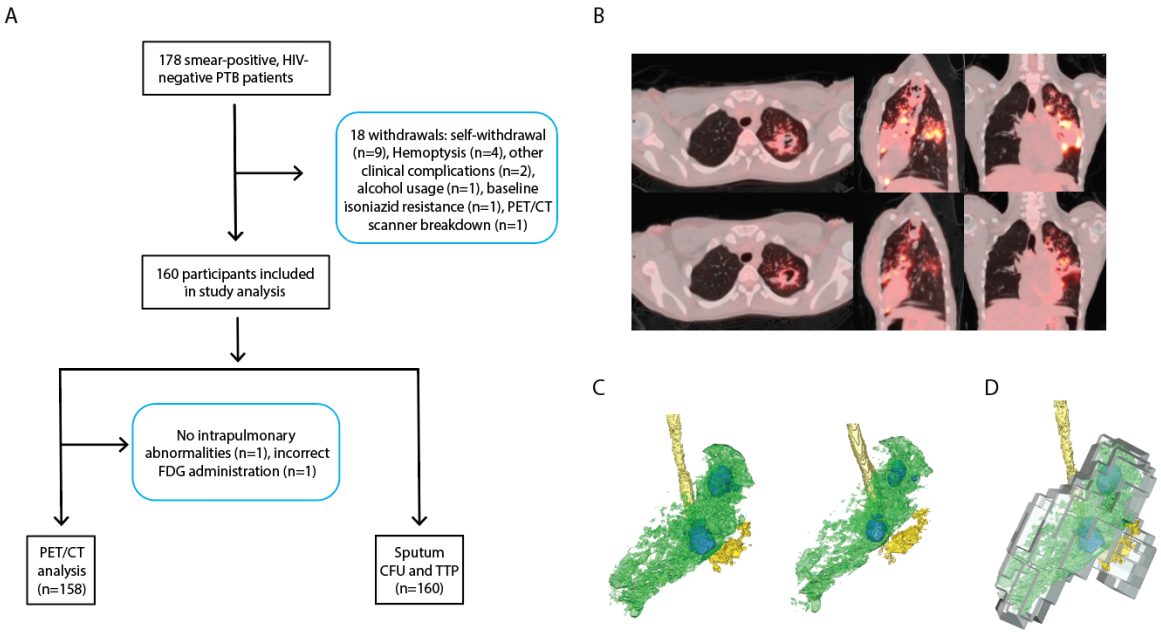

Fig. 1. Participant study flow and PET/CT scan analysis. A. Patient flow diagram for the study. B. Baseline (top) and day 14 (bottom) PET/CT scans for a patient in the isoniazid-rifampicin-pyrazinamide-ethambutol arm. In the axial view a slice through the large left apical cavity shows the typical cool liquified interior of a cavity in S1/S2 which is draining down into the lower segments of the superior lobe creating an area of consolidation highlighted in the coronal view on the right. The sagittal view in the center shows a second lesion in the apical segment (S6) of the inferior lobe. C. Three-dimensional rendering of the left lung showing the label fields encompassing the cavity and consolidation in the left superior lobe in green within which is the airspace in the cavity in red. The lower yellow lesion is in the inferior lobe segment S6. These are the lesions used in the primary analysis. D. Three-dimensional rendering of the 11x11x11 voxel co-registered cubes embedded within these lesions. These are the lesion cubes used in the exploratory analysis.

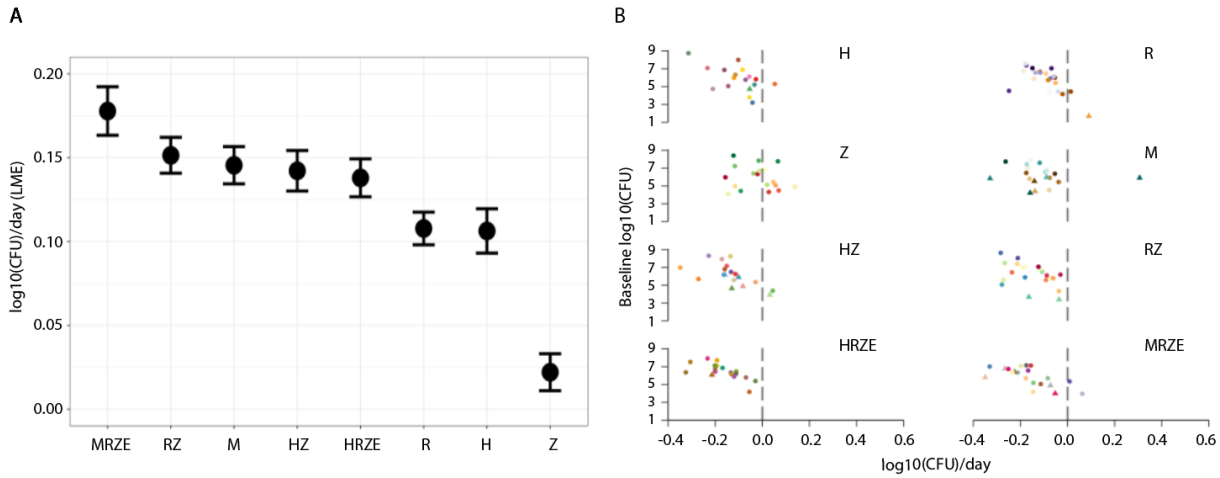

Fig. 2. Conventional early bactericidal activity (EBA) estimates. In A the arm-level effect was estimated using linear mixed effects modelling from daily overnight samples plated onto solid growth media. The Y-axis is the estimated daily log10 decrease in CFU for each arm and the error bars represent 95% confidence intervals on the estimate of the arm-level effect. B. Intraindividual variation in the estimated drug effect by arm, calculated as the slope of the line connecting log10(CFU) at baseline and log10(CFU) at Day 13. Each participant has a unique color coding, the Y-axis is the log10(CFU) of that participant at baseline. For those subjects without Day 13 data, we instead calculate the slope of the line connecting log10(CFU) at baseline and log10(CFU) at the last day on which that subject was measured; we denote these subjects with a triangle in-place of a circle. H=isoniazid, R=rifampicin, Z=pyrazinamide, E=ethambutol, M=moxifloxacin.

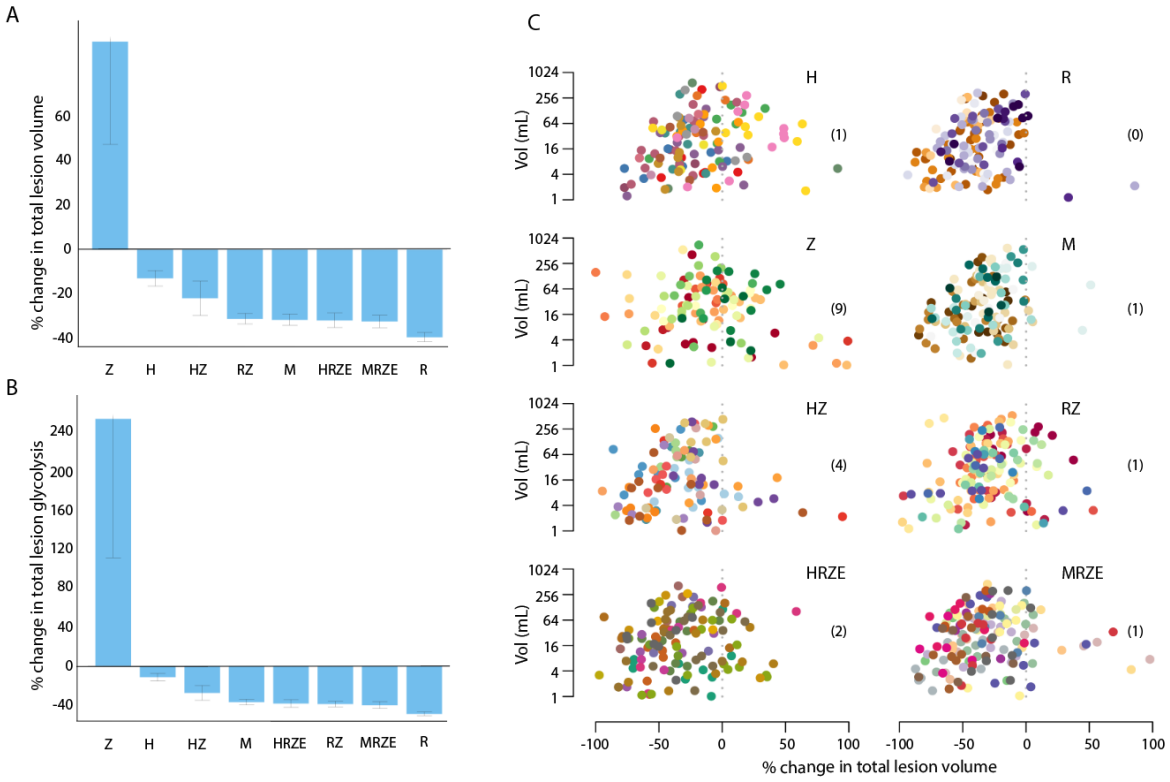

Fig. 3. Arm-level radiologic changes. (A) average percent changes in total lesion volume (-500HU to 200HU) and (B) total glycolytic activity were calculated for all lesions (N=763, 45 lesions were excluded from this analysis, reasons for these exclusions are detailed in Supplemental Table 2). Error bars are standard error of the mean. C. Total volume changes within individual lesions as a function of baseline lesion volume. Each subject is a unique color (same color scheme as Figure 2B) and contributes multiple lesions to the plot. Lesions that change more than 100% are not shown and the number omitted from each plot is given. H=isoniazid, R=rifampicin, Z=pyrazinamide, E=ethambutol, M=moxifloxacin.

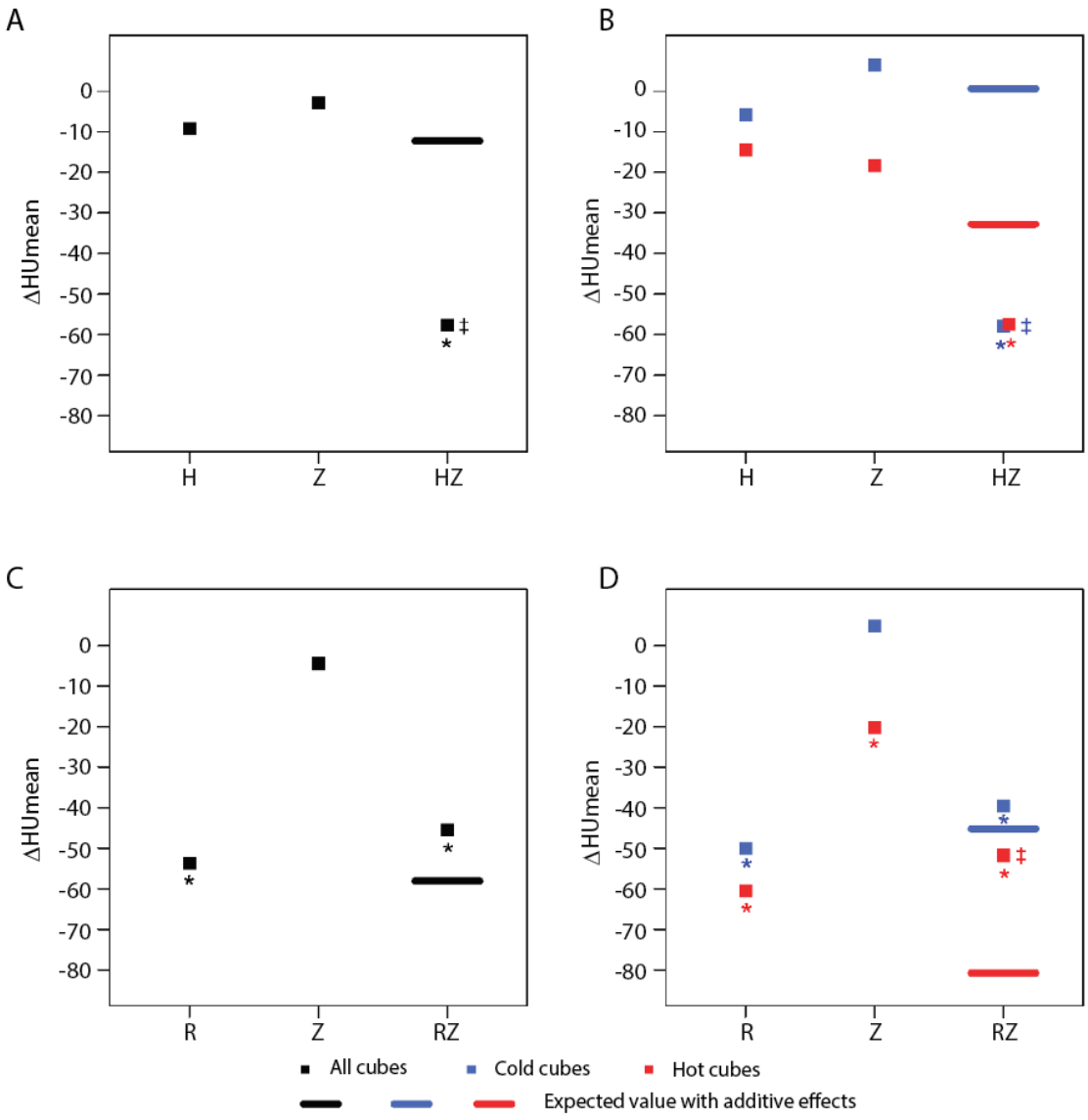

Fig. 4. Sub-lesion level changes. Lesions were divided into 1 cm3 cubes and baseline and day 14 cube sets were computationally aligned to produce 145,447 cube sets. A-D represent linear mixed effects modeling estimates of the change in HUmean for all cubes for subjects in the indicated arms. A and C show the result for all cubes while B and D show the results for hot cubes (SUVmean >2) and cold cubes (SUVmean <=2). The y-axis is the mean decrease in HU observed for all cubes and the vertical bars show the expected value if the individual estimates were summed. * indicates a significant change from baseline with P<0.05, ‡ indicates significant treatment interaction with a P value <0.05**.** H=isoniazid, R=rifampicin, Z=pyrazinamide.

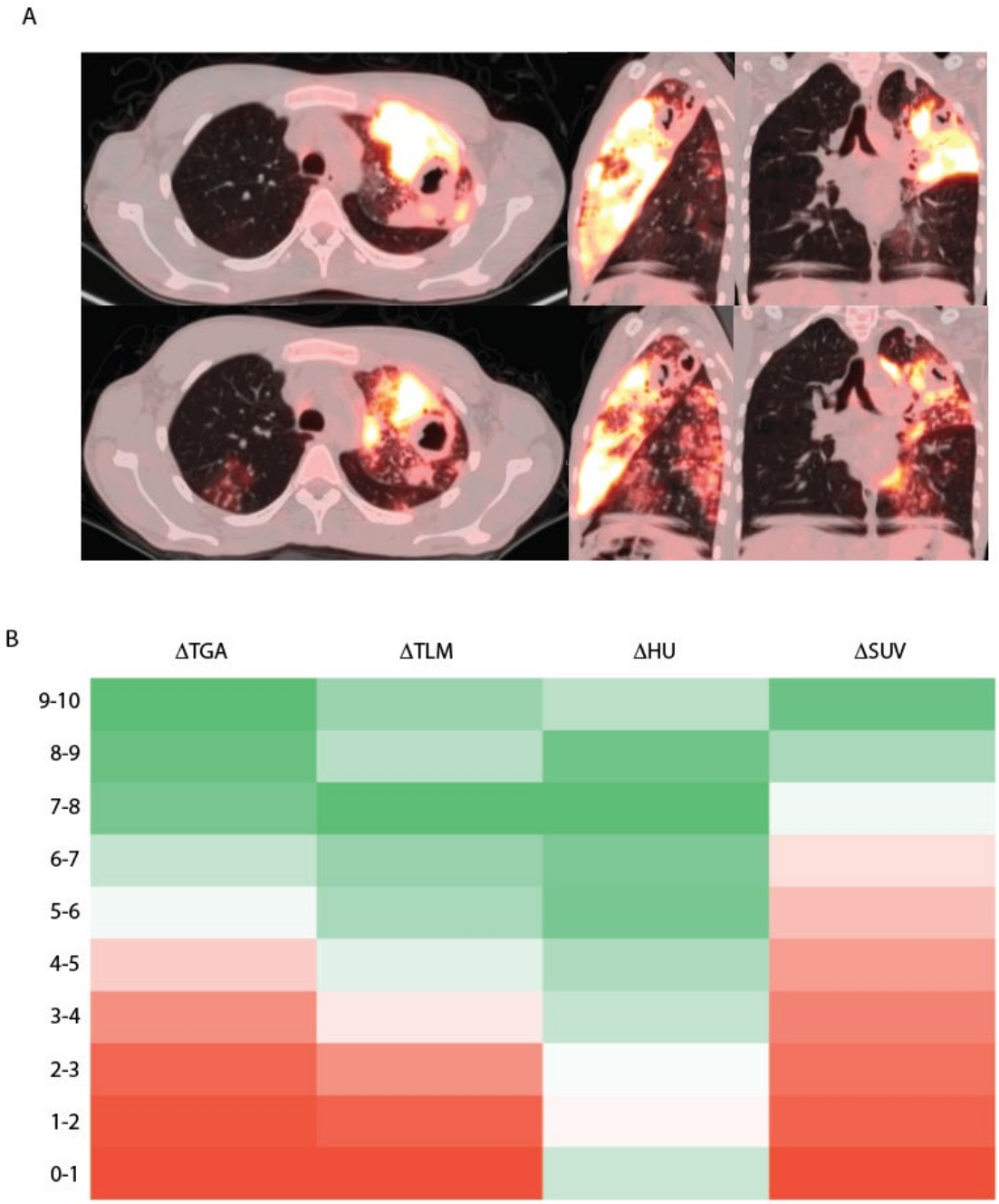

Fig. 5. Baseline inflammatory status and pyrazinamide activity. A. PET/CT scans of one participant receiving pyrazinamide monotherapy showing a large area of consolidation below a left apical cavity that shows a strong response to pyrazinamide reducing in both lesional volume and FDG avidity within the consolidation. Top scans are baseline and bottom are day 14. B. Heatmap of the 14,466 cubes extracted from all patients in the pyrazinamide arm arranged by baseline SUV (y-axis). The color reflects the extent of decrease (baseline-day 14) in TGA, TLM

(total lesion mass, the sum of all HU values + 1024 for each voxel within a cube), HUmean, and SUVmean. Green (maximum) is 61.5, average (white) is 24.6 and minimum (red) is -24.4 indicating cubes that worsened for each feature.

Supplementary Materials:

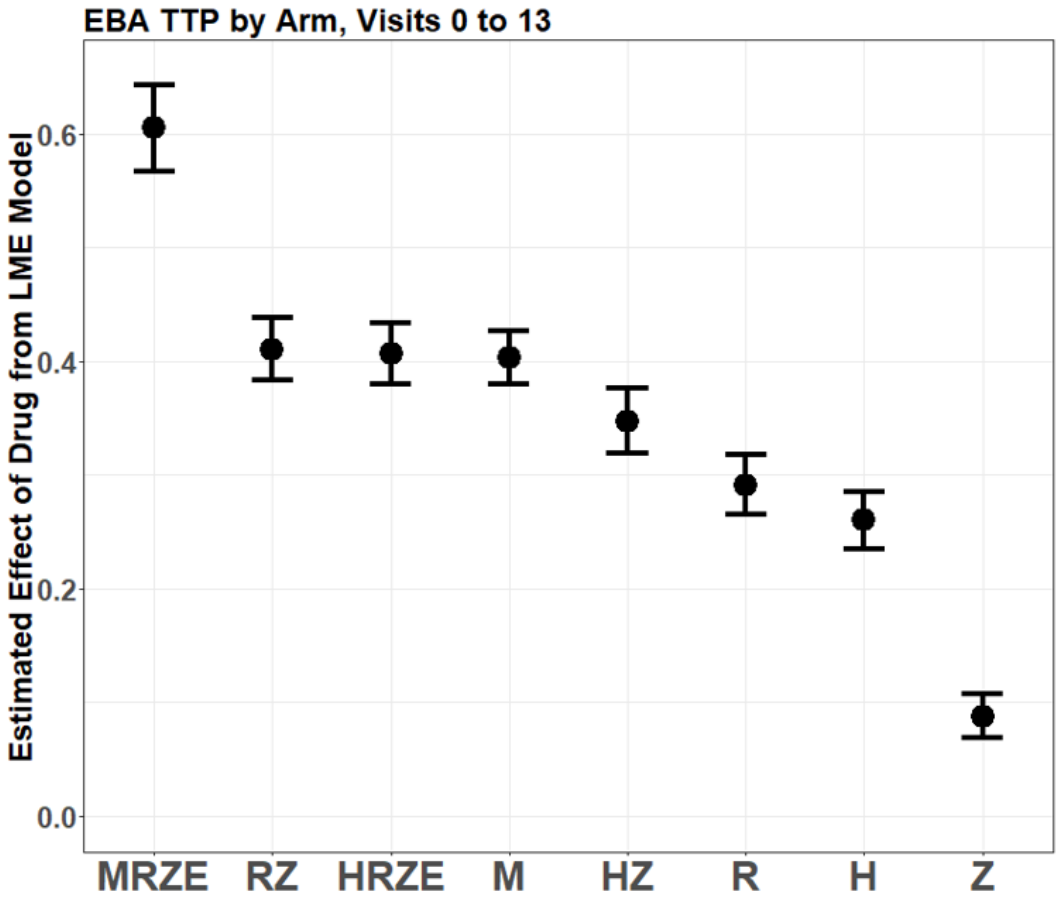

Fig. S1. Estimated EBA effect from time-to-positivity of cultures from the cultures in liquid broth medium according to the mycobacterial growth indicator tube system (BACTEC MGIT 960). H=isoniazid, R=rifampicin, Z=pyrazinamide, E=ethambutol, M=moxifloxacin.

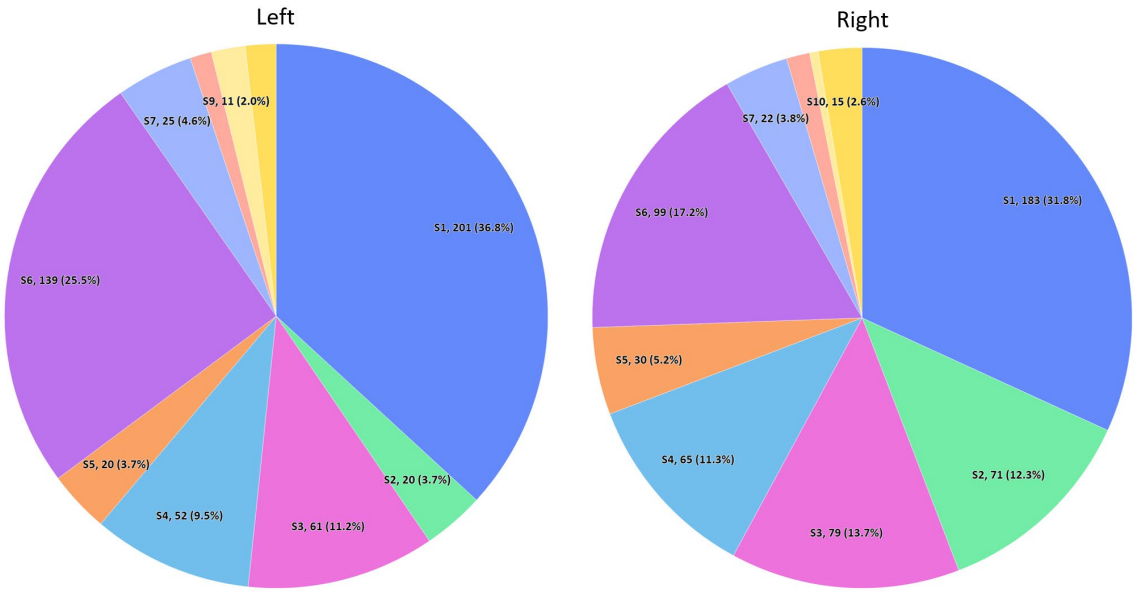

Fig. S2. Segmental distribution of annotated lesions (including cavitary air). The number and percentage represent the number of lesions that have the indicated location for the primary bronchopulmonary segment. Complex lesions involving multiple segments are only listed by their primary segment.

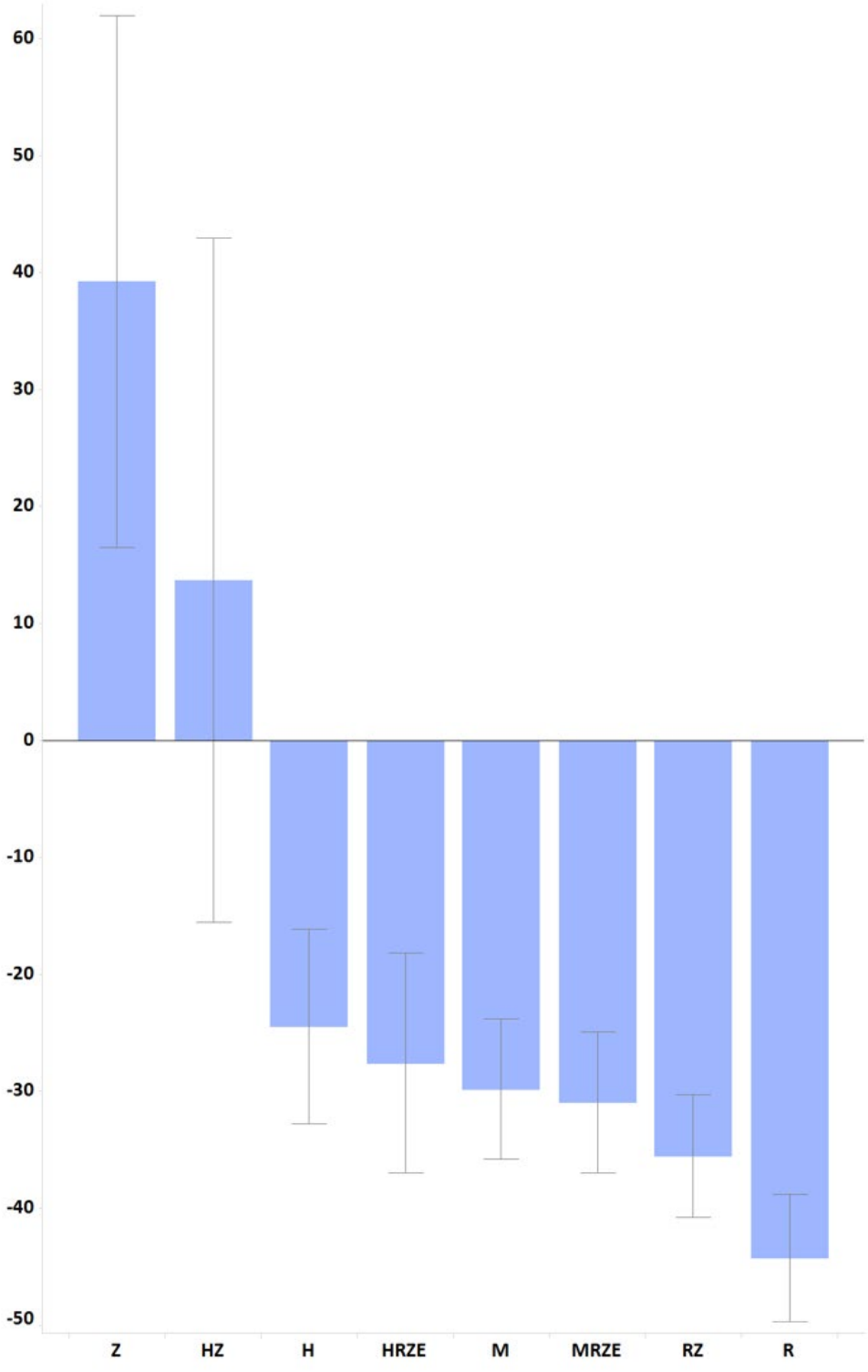

Fig. S3. Cavitary air percent change by arm. Average percent changes in features with radiodensity from -500 to -1024 HU (N=314, 6 cavitary air lesions were excluded from this analysis, reasons for these exclusions are detailed in Supplemental Table 2). Error bars are standard errors of the mean. H=isoniazid, R=rifampicin, Z=pyrazinamide, E=ethambutol, M=moxifloxacin.

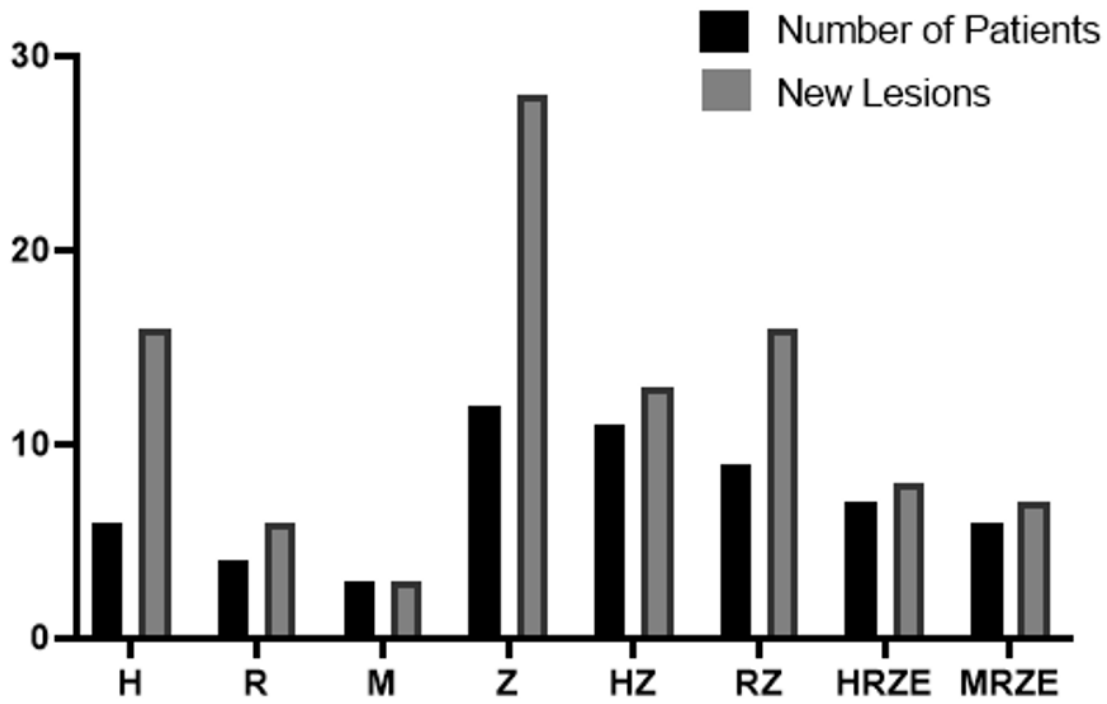

Fig. S4. Appearance of new or expanded lesions by study arm. The black bar shows the number of participants per arm that had new lesions, the grey bar shows the total number of new lesions. H=isoniazid, R=rifampicin, Z=pyrazinamide, E=ethambutol, M=moxifloxacin.

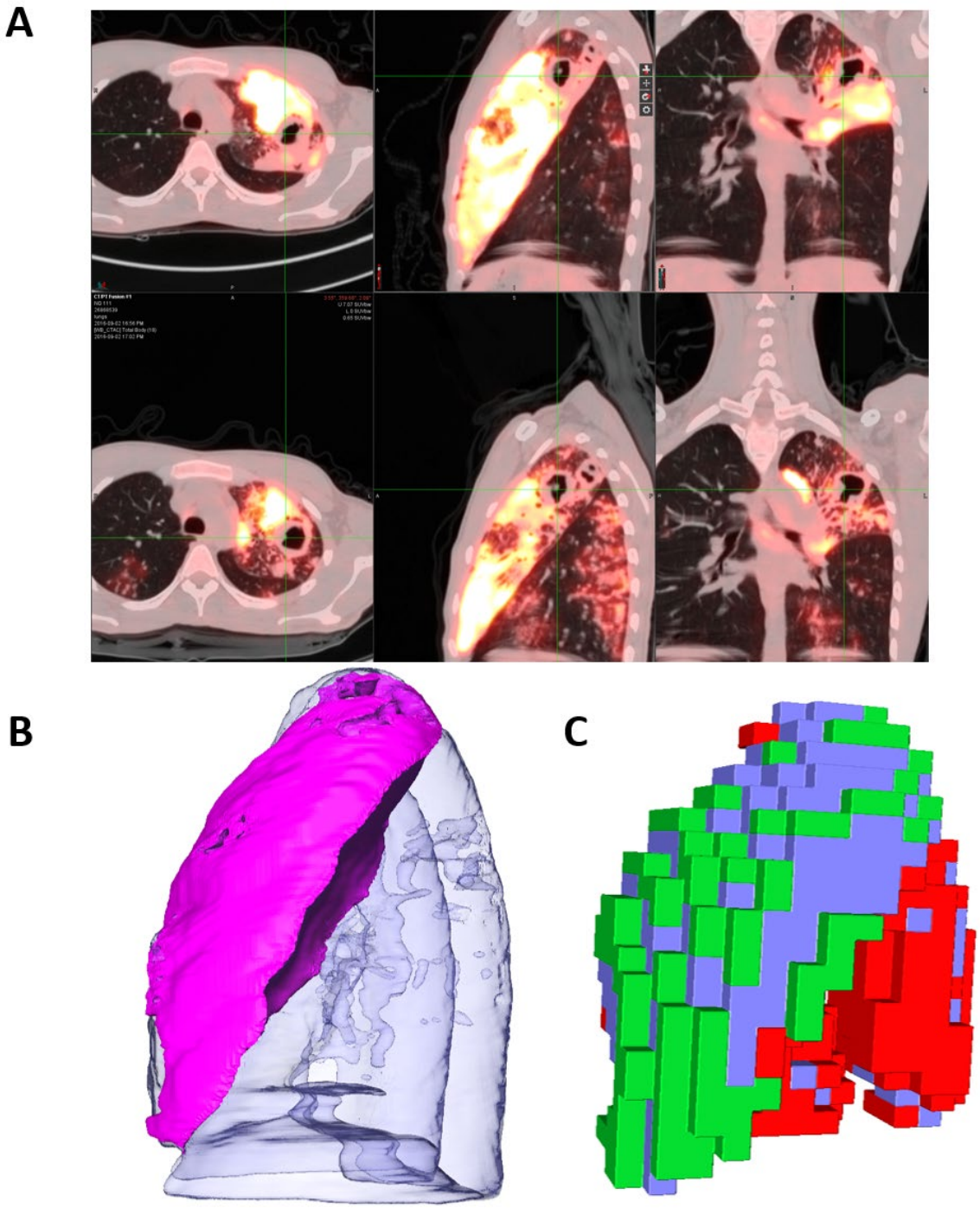

Fig. S5. Sub-lesion level analysis. **A**. PET/CT sections of diseased lung area in a participant with a large consolidation below a cavity in the left superior lobe. The consolidation shows a large response at day 14, decreasing in total glycolytic activity and lesional volume by over 40%. In contrast the left inferior lobe, which shows minimal disease at baseline, progresses significantly by day 14. **B.** Computational rendering of the superior lobe lesion. **C.** Surface representation of 1,100 11x11x11 voxel co-registered cubes across the entire left lung colored by whether they decrease in median HU (green), increase in median HU (red) or are unchanged (blue).

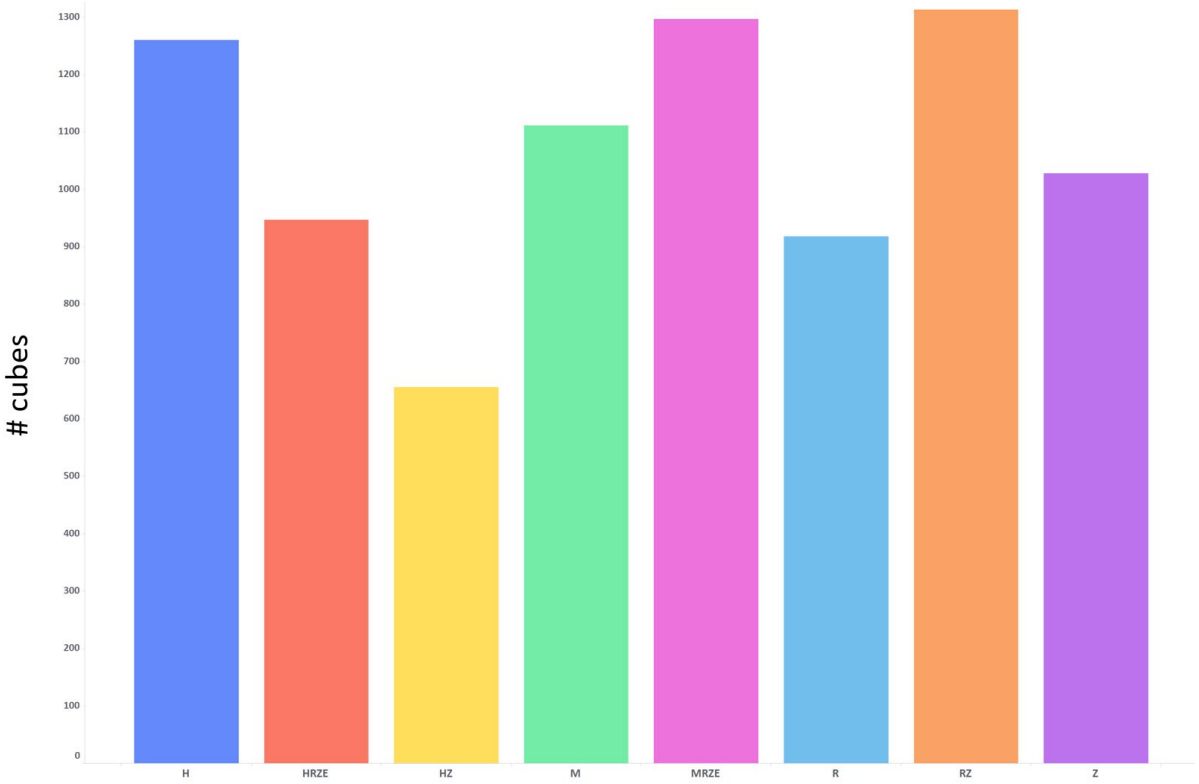

Fig. S6. Arm distribution of cubes that contained no lesion material at baseline N= 18,760 (radiodensity >-500HU or SUVmean <2) that represent new lesions resulting from bronchial spread of existing disease. These cubes were omitted from the outcome analysis. H=isoniazid, R=rifampicin, Z=pyrazinamide, E=ethambutol, M=moxifloxacin.

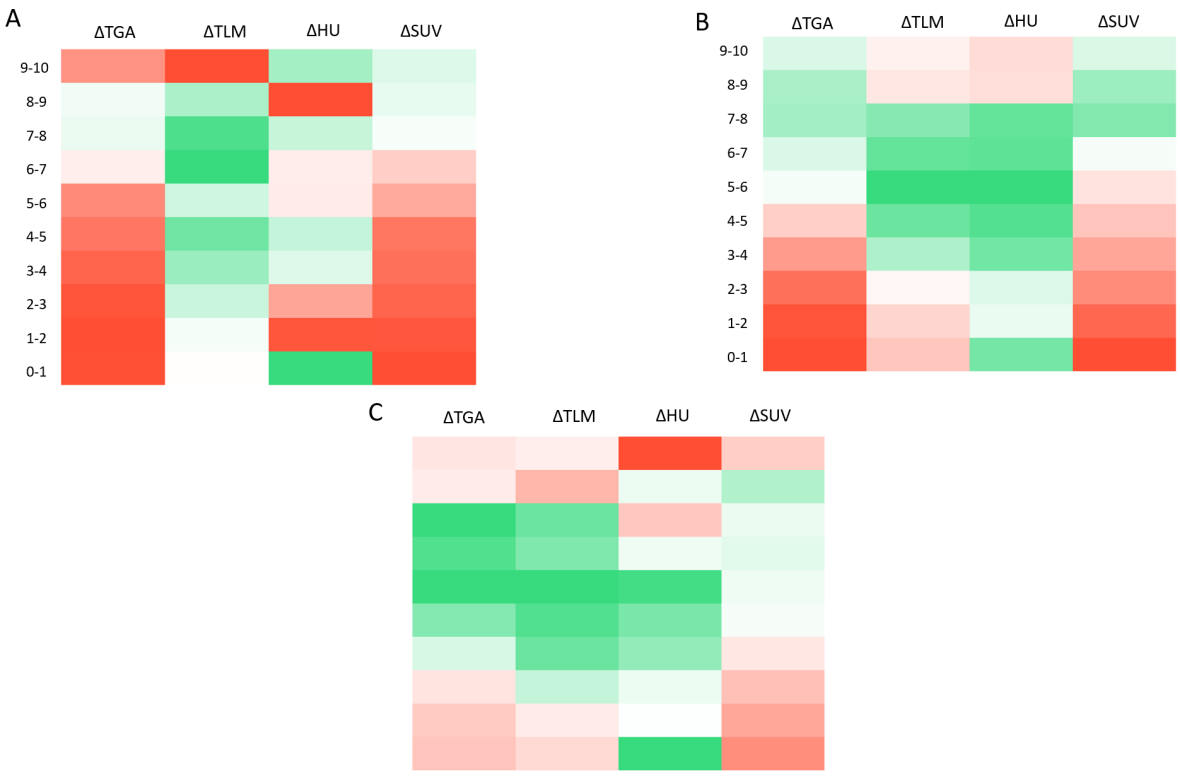

Figure S7. Cube-level response to individual agents stratified by baseline SUVmean values. A. Isoniazid. B. Rifampicin. C. Moxifloxacin

Table S1. Participant baseline characteristics

		All (n=160)	H (n=18)	R (n=21)	Z (n=19)	M (n=21)	RZ (n=23)	HZ (n=18)	HRZE (n=19)	MRZE (n=21)	p-values
Sex	Male N (%)	110 (68.8%)	14 (77.8%)	14 (66.7%)	14 (73.7%)	16 (76.2%)	18 (78.3%)	11 (61.1%)	13 (68.4%)	10 (47.6%)	0.440[1]
Age	Mean (Range)	32.4 (18.2-59.5)	31.4 (18.8-47.5)	33.0 (19.5-53.8)	30.4 (18.2-48.3)	32.6 (20.9-48.9)	30.5 (19.8-55.2)	29.4 (18.4-46.0)	35.2 (19.4-59.5)	36.7 (18.7-56.3)	0.338[2]
BMI	Mean (SD)	18.9 (3.3)	19.3 (3.3)	18.9 (1.9)	18.7 (3.1)	19.0 (4.4)	19.3 (4.1)	19.5 (4.3)	18.1 (2.3)	18.7 (1.8)	0.925[2]
Xpert cycle threshold	Mean (SD)	16.5 (4.2)	16.7 (3.6)	16.4 (4.8)	17.2 (4.1)	17.4 (5.5)	16.6 (5.2)	15.1 (3.2)	16.2 (2.7)	16.5 (3.8)	0837[2]
CFU (log10/ml sputum)	Mean (SD)	6.0 (1.2)	5.9 (1.4)	5.8 (1.4)	5.8 (1.3)	6.3 (1.1)	6.1 (1.4)	6.2 (1.3)	6.5 (0.9)	5.8 (1.1)	0.587[2]
Total lesion volume on CT	Mean (SD)	386.8 (286.1)	420.7 (247.8)	333.3 (242.3)	339.8 (209.4)	422.8 (447.5)	485.5 (322.1)	341.0 (327.0)	332.0 (169.3)	403.0 (217.5)	0.585[2]
Total dense lesion volume on CT	Mean (SD)	192.6 (159.7)	202.5 (156.4)	157.7 (108.2)	175.5 (165.9)	203.9 (203.3)	246.7 (193.6)	182.5 (174.7)	169.0 (115.2)	196.5 (141.3)	0.738[2]
Total soft lesion volume on CT	Mean (SD)	159.2 (116.0)	187.6 (148.2)	142.6 (120.1)	139.8 (69.9)	170.9 (172.1)	191.5 (121.6)	118.5 (81.2)	138.6 (79.2)	176.7 (86.6)	0.406[2]
Total glycolytic activity	Mean (SD)	1166.7 (875.8)	1296.6 (828.0)	976.6 (715.9)	1055.6 (870.1)	1203.9 (1053.3)	1481.3 (1099.7)	1000.0 (773.7)	1051.7 (832.0)	1226.5 (745.6)	0.589[2]
Total cavity air volume on CT	Mean (SD)	34.9 (61.4)	30.0 (41.1)	33.0 (51.7)	24.4 (41.9)	48.0 (91.4)	47.2 (66.8)	39.8 (102.8)	24.4 (18.8)	29.6 (32.8)	0.856[2]

[1]Fisher's exact test of any difference between the 8 arms
[2]ANOVA test of any difference between the 8 arms

Note: H=isoniazid, R=rifampicin, Z=pyrazinamide, E=ethambutol, M=moxifloxacin.

Table S2. Lesions excluded from lesion-level analysis

Subject	Lesion	Reason	Arm
NG_002	L_S1_S2_S3_S4_S5_LESION	No lung present, totally destroyed upper lobe	RZ
NG_010	R_S4_LESION	Old, calcified lesion - inactive	HRZE
NG_010	R_S1_S2_LESION	Fully collapsed upper lobe	HRZE
NG_010	R_S6	Pleural disease adjacent to existing lesion	HRZE
NG_017	R_S1_S2_LESION	Old, calcified lesion - inactive	HZ
NG_017	R_S2_AIR	Old, calcified lesion - inactive	HZ
NG_027	R_S6_LESION	Severe motion artifact	R
NG_047	R_S1_S2_S3_LESION	Accidentally duplicated in initial segmentation, combined into single R_S1_S2_S3 lesion	HRZE
NG_051	R_S3_LESION	Collapse, obvious septal distortion and left lung hyperinflated	Z
NG_054	R_S1_S2_LESION	No lung present, totally destroyed upper lobe	RZ
NG_064	L_S1_S2_LESION	Apical collapse of S1 and S2	R
NG_083	L_S1_S2_LESION	Old, calcified lesion - inactive	MRZE
NG_085	R_S1_S2_LESION	Old, calcified lesion - inactive	Z
NG_092	L_S4_LESION	New lesion spread from apical cavity, no sign of this at baseline	HRZE
NG_094	R_S3_LESION	Adjacent to a large lower lobe pleural effusion and segments are barely visible	M
NG_094	R_S4_LESION	Adjacent to a large lower lobe pleural effusion and segments are barely visible	M
NG_099	R_S6_S7_S8_S9_S10_LESION	New lesion spread from apical cavity, no sign of this at baseline	MRZE
NG_099	L_S3_LESION	New lesion spread from apical cavity, no sign of this at baseline	MRZE
NG_112	L_S6_S7_S8_S9_S10_LESION	Left lower lobe collapse	H
NG_112	L_S10_AIR	Airspace in collapsed lobe	H
NG_121	L_S1_S2_LESION	Old, calcified lesion - inactive	HZ
NG_131	L_S4_LESION	New lesion spread from apical cavity, no sign of this at baseline	HZ
NG_131	R_S3_LESION	New lesion spread from apical cavity, no sign of this at baseline	HZ
NG_150	R_S6_S8_S9_LESION	Large pleural effusion (S6,S8,S9)	Z
NG_150	R_S4_LESION	Small amount of pleural material R_S4	Z
NG_154	R_S1_S2_LESION	Old, calcified lesion - inactive	R

NG_157	R_S4_LESION	Old, calcified lesion - inactive	MRZE
NG_173	R_S4_S5_LESION	Large pleural effusion and middle lobe collapse	M
NG_174	R_S2_LESION	Old, calcified lesion - inactive	RZ
NG_175	L_S1_S2_S3_LESION	Left upper lobe collapse	RZ
NG_175	L_S1_AIR	Left upper lobe collapse	RZ
NG_180	R_S6_S9_S10_AIR	Bad reconstruction due to breath artifact	R
NG_180	R_S3	Cold pleural lesion	R
NG_183	L_S1_S2_LESION	Old, calcified lesion - inactive	HZ
NG_186	L_S6_LESION	Large pleural lesion	M
NG_199	R_S3_LESION	Old, calcified lesion - inactive	RZ
NG_206	R_S3	New lesion from apical cavity, no sign of this at baseline	HRZE
NG_217	L_S1_S2_LESION	Pleural expansion of existing lesion	MRZE
NG_220	L_S7_S8_LESION	Reconstruction artifact, small lesion near diaphragm	RZ
NG_231	R_S3_AIR	Airspace within old, inactive lesion	RZ
NG_236	L_S1_S2_S3_S4_S5_LESION	Complete collapse and erosion of left superior lobe	HZ
NG_236	L_S1_S2_S3_S4_S5_AIR	Airspace within collapsed lobe	HZ
NG_244	L_S6_LESION	Reconstruction artifact, small lesion near diaphragm	HZ
NG_250	R_S6_LESION	New lesion spread from apical cavity, no sign of this at baseline	RZ
NG_261	L_S1_S2_S3_LESION	Left upper lobe collapse	M

Note: H=isoniazid, R=rifampicin, Z=pyrazinamide, E=ethambutol, M=moxifloxacin.

Table S3. Inclusion and exclusion criteria.

Inclusion Criteria	**1.** Age 18 to 65 years with body weight from 30 kg to 90 kg **2.** Sputum acid-fast bacilli (AFB) smear positive (at least 1+ on the WHO—International Union Against Tuberculosis and Lung Disease scale) **3.** Likely able to produce approximately 10 mL of sputum per day **4.** Xpert MTB/RIF-confirmed *M.tb* **5.** Rifampin-sensitive pulmonary tuberculosis as indicated by Xpert MTB/RIF **6.** ALT <3X upper limit of normal, creatinine <2X upper limit of normal **7.** Willingness to have samples stored
Exclusion Criteria	**1.** Clinically suspected disseminated TB or acuity of illness too much as deemed by clinicians **2.** Has been treated for tuberculosis within the past 3 years **3.** Treatment with agents known to have anti-tuberculosis activity (e.g., fluoroquinolones, linezolid) for any indications during the current episode of clinical illness or within 2 months prior to screening, whichever is longer **4.** Cirrhosis or chronic kidney disease **5.** Disease complications or concomitant illness that might compromise safety or the interpretation of trial endpoints, such as known diagnosis of chronic inflammatory condition (e.g., sarcoidosis, rheumatoid arthritis, and connective tissue disorder) **6.** Use of immunosuppressive medications, such as TNF-alpha inhibitors or systemic or inhaled corticosteroids, within 2 weeks prior to screening **7.** Subjects with diabetes, point of care HbA1c above 6.5, or random glucose over 200 mg/dL **8.** Conditions which compromise the subject's ability to take or absorb oral drugs **9.** Normal PA-Chest radiograph, determined during screening **10.** Total lung (left or right) collapse on PA-Chest radiograph **11.** HIV positive **12.** Pregnant or breastfeeding **13.** Any other condition that, in the responsible clinician's judgment, renders a subject too sick to safely tolerate 2 weeks study therapy **14.** Any condition that constitutes a contraindication to any of the drugs to be used on any study arms

Supplemental statistical modeling methods

LMER Model summary.

Par1: HZ vs. H and HZ vs. Z

Model 1: no interaction term – Fixed-effect estimates

model formula: HUMEAN change ~ ARM + (1|PID/LESIONID)

	Estimate	Std. Error	df	t value	Pr(>|t|)
(Intercept)	-57.69956	10.93571	51.28915	-5.276253	0.0000027
ARMpza	54.76622	14.96912	48.94243	3.658614	0.0006201
ARMH	48.38528	15.15781	47.95343	3.192102	0.0024938

Variance-covariance matrix

3 x 3 Matrix of class "dpoMatrix"

	(Intercept)	ARMpza	ARMH
(Intercept)	119.59	-119.59	-119.59
ARMpza	-119.59	224.07	119.59
ARMH	-119.59	119.59	229.76

Model 2: no interaction term and no intercept model – Fixed-effect estimates

model formula: HUMEAN change ~ ARM -1 + (1|PID/LESIONID)

	Estimate	Std. Error	df	t value	Pr(>|t|)
ARMHZ	-57.699561	10.93570	51.28917	-5.2762546	0.0000027
ARMpza	-2.933338	10.22178	46.43788	-0.2869694	0.7754124
ARMH	-9.314280	10.49617	44.66574	-0.8873982	0.3796181

Variance-covariance matrix

3 x 3 Matrix of class "dpoMatrix"

	ARMHZ	ARMpza	ARMH
ARMHZ	119.59	0.00	0.00
ARMpza	0.00	104.48	0.00
ARMH	0.00	0.00	110.17

Model 3 – Fixed-effect estimates

model formula: HUMEAN change ~ ARM*HotCold + (1|PID/LESIONID)

	Estimate	Std. Error	df	t value	Pr(>|t|)
(Intercept)	-57.920209	11.043672	53.27642	-5.2446515	0.0000028
ARMpza	64.444109	15.102745	50.72828	4.2670460	0.0000866
ARMH	52.028794	15.276983	49.50240	3.4056982	0.0013175
HotCold	0.410160	4.072253	40808.39176	0.1007207	0.9197727

ARMpza:HotCold	-25.265093	5.464410	41713.83470	-4.6235718	0.0000038
ARMH:HotCold	-8.972115	5.211992	41452.29827	-1.7214368	0.0851790

Variance-covariance matrix

6 x 6 Matrix of class "dpoMatrix"

	(Intercept)	ARMpza	ARMH	HotCold	ARMpza:HotCold	ARMH:HotCold
(Intercept)	121.96	-121.96	-121.96	-6.58	6.58	6.58
ARMpza	-121.96	228.09	121.96	6.58	-11.68	-6.58
ARMH	-121.96	121.96	233.39	6.58	-6.58	-10.74
HotCold	-6.58	6.58	6.58	16.58	-16.58	-16.58
ARMpza:HotCold	6.58	-11.68	-6.58	-16.58	29.86	16.58
ARMH:HotCold	6.58	-6.58	-10.74	-16.58	16.58	27.16

Model 4: no intercept model – Fixed-effect estimates

model formula: HUMEAN change ~ ARM*HotCold -1 + (1|PID/LESIONID)

	Estimate	Std. Error	df	t value	Pr(>|t|)
ARMHZ	-57.920209	11.043672	53.27642	-5.2446515	0.0000028
ARMpza	6.523899	10.301953	48.00830	0.6332682	0.5295638
ARMH	-5.891415	10.555735	45.79120	-0.5581246	0.5794781
HotCold	0.410160	4.072253	40808.39174	0.1007207	0.9197727
ARMpza:HotCold	-25.265093	5.464410	41713.83469	-4.6235718	0.0000038
ARMH:HotCold	-8.972115	5.211992	41452.29826	-1.7214368	0.0851790

Variance-covariance matrix

6 x 6 Matrix of class "dpoMatrix"

	ARMHZ	ARMpza	ARMH	HotCold	ARMpza:HotCold	ARMH:HotCold
ARMHZ	121.96	0.00	0.00	-6.58	6.58	6.58
ARMpza	0.00	106.13	0.00	0.00	-5.10	0.00
ARMH	0.00	0.00	111.42	0.00	0.00	-4.16
HotCold	-6.58	0.00	0.00	16.58	-16.58	-16.58
ARMpza:HotCold	6.58	-5.10	0.00	-16.58	29.86	16.58
ARMH:HotCold	6.58	0.00	-4.16	-16.58	16.58	27.16

Estimated mean values:

Condition	Contrast	Estimate	Std	Wald Test

			Error	
	R	-53.63	8.37	-6.41
	Z	-4.43	8.54	-0.52
	RZ	-45.45	8.12	-5.60
	RZ-Z	-41.02	11.78	-3.48
	RZ-R	8.19	11.66	0.70
	(RZ-R)-(Z-0)	12.62	14.46	0.87
HOT	R	-60.58	8.75	-6.92
HOT	Z	-20.15	8.89	-2.27
HOT	RZ	-51.74	8.3	-6.23
HOT	RZ-Z	-31.59	12.16	-2.60
HOT	RZ-R	8.84	12.06	0.73
HOT	(RZ-R)-(Z-0)	28.99	14.98	1.97
COLD	R	-50.07	8.49	-5.90
COLD	Z	4.86	8.68	0.56
COLD	RZ	-39.62	8.28	-4.79
COLD	RZ-Z	-44.47	11.99	-3.71
COLD	RZ-R	10.45	11.85	0.88
COLD	(RZ-R)-(Z-0)	5.59	14.69	0.38
HOT vs COLD	H:(RZ-R)-(Z-0) - C:(RZ-R)-(Z-0)	23.39	6.3	3.71

Part 2: RZ vs. R and RZ vs. Z

Model 1: no interaction term – Fixed-effect estimates

model formula: HUMEAN change ~ ARM + (1|PID/LESIONID)

	Estimate	Std. Error	df	t value	Pr(>|t|)
(Intercept)	-45.447814	8.116425	58.46323	-5.5994870	0.0000006
ARMpza	41.021327	11.784374	58.07175	3.4809934	0.0009552
ARMR	-8.186288	11.661351	55.79444	-0.7020017	0.4855964

Variance-covariance matrix

3 x 3 Matrix of class "dpoMatrix"

	(Intercept)	ARMpza	ARMR
(Intercept)	65.88	-65.88	-65.88
ARMpza	-65.88	138.87	65.88
ARMR	-65.88	65.88	135.99

Model 2: no interaction term and no intercept model – Fixed-effect estimates

model formula: HUMEAN change ~ ARM -1 + (1|PID/LESIONID)

	Estimate	Std. Error	df	t value	Pr(>|t|)
ARMRZ	-45.447815	8.116430	58.46314	-5.5994831	0.0000006
ARMpza	-4.426479	8.543724	57.72094	-0.5180972	0.6063708
ARMR	-53.634092	8.373223	53.42319	-6.4054295	0.0000000

Variance-covariance matrix

```
3 x 3 Matrix of class "dpoMatrix"
      ARMRZ ARMpza  ARMR
ARMRZ  65.88      0  0.00
ARMpza  0.00     73  0.00
ARMR    0.00      0 70.11
```

Model 3 – Fixed-effect estimates

model formula: HUMEAN change ~ ARM*HOtCold + (1|PID/LESIONID)

	Estimate	Std. Error	df	t value	Pr(>|t|)
(Intercept)	-39.617330	8.275393	62.14814	-4.7873654	0.0000108
ARMpza	44.472340	11.991143	61.09407	3.7087658	0.0004514
ARMR	-10.449661	11.854872	58.43295	-0.8814655	0.3816774
HotCold	-12.124269	3.190653	47094.94183	-3.7999337	0.0001449
ARMpza:HotCold	-12.876992	4.999396	46680.07226	-2.5757094	0.0100065
ARMR:HotCold	1.613236	4.984089	46355.09858	0.3236773	0.7461838

Variance-covariance matrix

```
6 x 6 Matrix of class "dpoMatrix"
             (Intercept) ARMpza   ARMR HotCold ARMpza:HotCold
(Intercept)        68.48 -68.48 -68.48   -4.92          4.92
ARMpza            -68.48 143.79  68.48    4.92        -10.45
ARMR              -68.48  68.48 140.54    4.92         -4.92
HotCold            -4.92   4.92   4.92   10.18        -10.18
ARMpza:HotCold      4.92 -10.45  -4.92  -10.18         24.99
ARMR:HotCold        4.92  -4.92  -9.98  -10.18         10.18
             ARMR:HotCold
(Intercept)          4.92
ARMpza              -4.92
ARMR                -9.98
HotCold            -10.18
ARMpza:HotCold      10.18
ARMR:HotCold        24.84
```

Model 4: no intercept model – Fixed-effect estimates

model formula: HUMEAN change ~ ARM*HotCold -1 + (1|PID/LESIONID)

	Estimate	Std. Error	df	t value	Pr(>|t|)
ARMRZ	-39.617328	8.275394	62.14809	-4.7873643	0.0000108
ARMpza	4.855020	8.677869	60.15728	0.5594714	0.5779172
ARMR	-50.066980	8.488575	55.17188	-5.8981610	0.0000002
HotCold	-12.124268	3.190653	47094.94163	-3.7999335	0.0001449
ARMpza:HotCold	-12.876991	4.999396	46680.07178	-2.5757093	0.0100065
ARMR:HotCold	1.613235	4.984089	46355.09782	0.3236771	0.7461840

6 x 6 Matrix of class "dpoMatrix"

	ARMRZ	ARMpza	ARMR	HotCold	ARMpza:HotCold	ARMR:HotCold
ARMRZ	68.48	0.00	0.00	-4.92	4.92	4.92
ARMpza	0.00	75.31	0.00	0.00	-5.53	0.00
ARMR	0.00	0.00	72.06	0.00	0.00	-5.06
HotCold	-4.92	0.00	0.00	10.18	-10.18	-10.18
ARMpza:HotCold	4.92	-5.53	0.00	-10.18	24.99	10.18
ARMR:HotCold	4.92	0.00	-5.06	-10.18	10.18	24.84

Condition	**Contrast**	**Estimate**	**Std Error**	**Wald Test**
	H	-9.31	10.5	-0.89
	Z	-2.93	10.22	-0.29
	HZ	-57.7	10.94	-5.28
	HZ-Z	-54.77	14.97	-3.66
	HZ-H	-48.39	15.16	-3.19
	(HZ-H)-(Z-0)	-45.46	18.28	-2.49
HOT	H	-14.45	10.66	-1.36
HOT	Z	-18.34	10.45	-1.76
HOT	HZ	-57.51	11.2	-5.13
HOT	HZ-Z	-39.17	15.32	-2.56
HOT	HZ-H	-43.06	15.46	-2.79
HOT	(HZ-H)-(Z-0)	-24.72	18.66	-1.32
COLD	H	-5.89	10.56	-0.56
COLD	Z	6.52	10.3	0.63
COLD	HZ	-57.92	11.04	-5.24
COLD	HZ-Z	-64.44	15.1	-4.27
COLD	HZ-H	-52.03	15.28	-3.41
COLD	(HZ-H)-(Z-0)	-58.55	18.43	-3.18
HOT vs COLD	H:(HZ-H)-(Z-0) - C:(HZ-H)-(Z-0)	33.83	6.36	5.32

Note: H=isoniazid, R=rifampicin, Z=pyrazinamide, E=ethambutol, M=moxifloxacin.